UNDERSTANDING CELLULAR DYNAMICS OF DROSOPHILA AND MOUSE GERMLINE THROUGH ADVANCED IMAGING AND ANALYSIS

by

KARL A. KUDYBA

(Under the Direction of Cordula Schulz)

ABSTRACT

The germline represents the future of all metazoan species. In the male, reproductive success has largely been attributed to the ability to produce vast quantities of gametes specially adapted for motility. In order to achieve such a feat, a stem cell must both maintain a constant supply of differentiating daughters and consistently self-renew. This thesis applies modern techniques, utilizing two model organisms, to further our understanding and ability to study the cells responsible for germline renewal. The first manuscript presented addresses the complex architecture of the mouse testis through the use tissue clearing and light-sheet microscopy. An assessment of this approach is accomplished through the staining of a well characterized population. Measurement of tissue arrangement is achieved through computer recognition of signal and background features. The paper concludes with validation of putative labels of stem cell populations. A second manuscript uses the fruit fly to investigate the effects of persistent mating on germline stem cells. A mating induced increase in the mitotic activity of these cells is shown to be dependent on G-protein signaling.

The presented research provides new avenues of study in the germline; increasing the tools available in mammalian tissues and uncovering signal pathways regulating division in *Drosophila*.

INDEX WORDS: Germline, Stem Cell, Spermatogonia, Testis, Light-Sheet Microscopy, *Drosophila*, Mouse, Tissue Clearing

UNDERSTANDING CELLULAR DYNAMICS OF DROSOPHILA AND MOUSE GERMLINE THROUGH ADVANCED IMAGING AND ANALYSIS

by

KARL A. KUDYBA

BS, Southern Polytechnic State University, 2011

A Dissertation Submitted to the Graduate Faculty of The University of Georgia in Partial Fulfillment of the Requirements for the Degree

DOCTOR OF PHILOSOPHY

ATHENS, GEORGIA

2019

UNDERSTANDING CELLULAR DYNAMICS OF DROSOPHILA AND MOUSE GERMLINE THROUGH ADVANCED IMAGING AND ANALYSIS

by

KARL A. KUDYBA

Major Professor: Cordula Schulz
Committee: James Lauderdale
Douglas Menke
Jonathan Eggenschwiler

Electronic Version Approved:

Ron Walcott

Interim Dean of the Graduate School

The University of Georgia

December 2019

DEDICATION

This thesis is dedicated to my parents (Georjan and Paul Kudyba), my wife (Heather Kudyba), and my son (Lukas Kudyba).

TABLE OF CONTENTS

Page

LIST OF TABLES

Page

LIST OF FIGURES

Page

CHAPTER 1

INTRODUCTION AND LITERATURE REVIEW

1.1 Spermatogenesis:

Spermatogenesis is the process by which the motility specialized male gamete is produced for the transmittance of genetic information across a distance. At the root of this, lies a stem cell pool responsible for propagation of the entire germline lineage. The fertility and fitness of an individual is dependent on the ability to derive vast quantities of sperm from this relatively small population[1,2]. Generally, sperm production begins with the asymmetric division of a stem cell resulting in both a new stem cell and a daughter cell beginning the process of differentiation. The latter daughter conducts a series of amplifications, consisting of cellular divisions and incomplete cytokinesis. This results in a chain of germline connected by intercellular bridges, known as a syncytium. After a species-specific number of mitotic divisions, the syncytial cluster will altogether undergo meiosis, ultimately resulting in haploid gametes. Lastly, a morphological restructuring of the cell, spermiogenesis, is undertaken to produce highly motile sperm[2].

1.2 Mammalian/Mouse spermatogenesis:

1.2.1 Testicular morphology

Murine testes have long been used as a model of mammalian spermatogenesis. Though slight variation in cell-type characteristics exist

between rodents and primates, much of the structure, molecular signaling, and germline progression have proven to be analogous[3]. The mammalian testis consists of a fibrous capsule, the tunica albuginea, enclosing a convoluted network of seminiferous tubules connected terminally to collecting ducts known as the rete testis[4]. Interstitial to the seminiferous tubules are a branching web of vasculature, nerves, macrophages, and hormone producing Leydig cells. The seminiferous tubule is enclosed by peritubular myoid cells which maintain a basement membrane on the internal margin. Sperm production takes place within the seminiferous tubule between the supportive, somatic Sertoli cells in a marginal to luminal fashion. The mammalian germline lineage consists broadly of mitotically active spermatogonia, meiotic spermatocytes, haploid spermatids, and the motility adapted spermatozoa (Figure 1.1A)[5–9].

1.2.2 Expansion and organized timing

The asynchronous division between, and clonal expansion of germline populations, along with the timed advancement of spermatogenesis, results in the regularly spaced occurrence of specific cell-types linearly through a tubule. These distinct distributions have been characterized into the seminiferous cycle; a series of repeating stages developed based on acrosomal development during spermiogenesis. The number of stages vary between mammalian species based on mitotic activity and size of stem cell pool. Resultant from this wave-like manner of differentiation, sperm production occurs in a continuous manner[10,11]. Mouse spermatogenesis can be split into twelve stages (I-XII), with individual tubule cross-sections classifying as a single stage(Figure 1.1A, B)[11].

Advancement of each stage has been timed through lineage tracing, with the entire cycle in mouse taking place across 8.6 days. The production of spermatozoa from spermatogonia occurs across 4 cycles requiring approximately 35 days[12,13].

The timing and progression of the seminiferous cycle is governed by the vitamin A metabolite, retinoic acid (RA)[6,14]. Withholding this signal prevents spermatogenic progression leaving only spermatogonia[15]. In doing so, synchronization (loss of the wave-like seminiferous cycle) can be achieved through external supplementation. Spermatogenesis resumes amongst the entire spermatogonia population, regardless of longitudinal location[16].

Significantly, the presence of RA between stages VI to IX mark key populational transitions in a wild-type animal. Within this timeframe, primitive spermatogonia transition from sporadic to programmatic divisions. Meiotic induction occurs within competent spermatogonia causing the progression of these cells luminally. Spermiation also takes place, resulting in the release of mature spermatozoa and the start of elongation in another generation of spermatids[6].

1.2.3 Heterogeneity of spermatogonia

Spermatogonia situate along the periphery of the seminiferous tubule and represent the most primitive germline cell-type in the adult. These cells are sequestered from the later lineages by tight junctions between adjacent Sertoli cells often referred to as the blood-testis barrier. In the rodent, staining of histological sections first subdivided spermatogonia into three distinct types based on nuclear profile: type A (SPG_A), intermediate (SPG_{In}), and type B

(SPG_B). It was further elucidated that the earliest lineage of spermatogonia, type A, exist in varying states of differentiation. Amongst SPG_A, a heterochromatin absent undifferentiated population (A_{undiff}) consists of single cells (A_s) and varying lengths of syncytia delineated as pairs (A_{pr}) and aligned chains of four, eight, or sixteen interconnected spermatogonia ($A_{al4\text{-}16}$)[9]. These A_{undiff} have shown to have preferential localization to the interstitial adjacent regions of the tubule, i.e. the SSC niche[17].

Most A_{undiff} transition without division to a differentiated state (A_1) at stage VII and enact a regimented series of three divisions resulting in A_2, A_3, and A_4 spermatogonia. A final pair of mitotic events marks the differentiation of SPG_A to SPG_{In} to SPG_B, which remain poised for meiotic entry. Entrance into meiosis is accompanied by a migration of the SPG_B through Sertoli-Sertoli tight junctions and into the luminal compartment. Accounting for the twice squared growth in population during meiosis, the expansion an A_s clone potentiates a maximum 4096 sperm.[5,9] However, apoptosis in the differentiated SPG_A makes this an infrequent occurrence[18].

Since the initial histological characterization of A_{undiff}, an increasingly diverse set of molecular markers have been found to label, exclude, or further subdivide the population. c-Kit, a tyrosine kinase receptor, is required for the migration of primordial germ cells in the developing embryo (Figure 1.2)[19]. In the adult, expression isolates the differentiating spermatogonia becoming detectable in A_1[20]. Octamer-4 (OCT4) a Yamanaka factor for inducing pluripotency, has been shown to mark most if not all of SPG_A in the adult mouse[21,22]. Promyelocytic

leukemia zinc finger protein (ZBTB16; PLZF)(Figure 1.2)[23–26], spalt-like 4(SALL4)[25–27], undifferentiated embryonic cell factor 1(UTF1)[28], neuregulin 3 (NGN3)[29], and LIN28A[30] all are restricted to the majority of the A_{undiff} population. RET and its correceptor, GDNF family receptor alpha 1 (GFRα1), are present in A_s to A_{al4} cells in apparent juxtaposition to NGN3 which becomes expressed in the partially differentiating $A_{al4\text{-}16}$ (Figure 1.2) [31–33].

Recently, several markers have been shown to define portions of the A_s cells. Inhibitor of DNA binding 4 (ID4) positive cells make up 4,000-6,000 of the estimated 35,000 A_s that populate an adult mouse testis [34–36]. ID4 labeling is thought to be isolated to SSCs within the A_{undiff}, though it is also expressed in a small subset of A_{pr}, believed to be a transient population (Figure 1.2). In the adult, ID4 is also present in late-stage primary spermatocytes and spermatids[34]. Paired box 7 (PAX7) is further restricted to approximately 400 cells within the A_s pool. These cells have been shown to be highly proliferative in contrast to the A_s population as a whole[37]. Notably the above markers are not exhaustive, with many more further contributing to spermatogonia heterogeneity. To date, no marker by itself has been universally considered to identify the SSC alone.

1.2.4 Extrinsic regulation of SSC maintenance and division

The hypothalamic-pituitary-gonadal axis (HPG) is an endocrine network between brain and gonadal structures. In the male gonadotropin-releasing hormone (GnRH) signals from the hypothalamus, for the release of follicle stimulating hormone (FSH) from the pituitary. FSH is conducted via vasculature to the testis where it acts on Leydig cells for the secretion of testosterone, which

feeds back to the brain and inhibiting further FSH secretion. FSH acts on both the spermatogonia and Sertoli cells while testosterone acts through Sertoli cells as the androgen receptor has yet to be detected in A_{undiff}[38–41].

Lack of a clear niche has hindered study of SSCs on a more local level, but study of the factors that allow for *in vitro* culture have given insight to the governing signals. The A_{undiff} have clear adherence to the basement membrane and thus can be isolated by differential plating on a layer of laminin[42]. Alternatively, many surface markers or reporters exist for a fluorescence-activated cell sorting approach[43]. The GFRα1 ligand, GDNF, is required for the long-term culture and expansion of isolated SSCs. This has been shown to act through Co-receptor RET and Src kinase family members in a phosphoinositide3 kinase dependent manner[44,45]. Fibroblast growth factor (FGF) are effective mitogens used in culture, that have been shown to act on A_{undiff} in an Erk1/2 dependent manner *in vivo*[46,47].

1.2.5 Models of spermatogonial stem cell renewal

The A_{undiff} have a clear pattern of clonal expansion from A_s to A_{al16}[9]. This paradigm led to a long-standing model proposing that the A_s population, in its entirety, represented the SSC pool. The A single model, as it is known, dictates an A_s would either complete cytokinesis during mitosis resulting in self-renewal, or its fellow daughters would remain coupled, becoming an A_{pr} and beginning differentiation[48]. Recent analyses have shown greater behavioral complexity than the A_s model allows[49].

Live imaging of GFRα1^{+} cells has demonstrated that early aligned syncytia can fragment, with one or more cells completing cytokinesis[50]. This suggests an ability to for A_{undiff} to revert to more simplified states potentially producing new SSCs. Furthermore, differentiating A_{undiff} cells, harboring a NGN3 pulse label, have shown the capability to revert identity to a more stem cell-like state and be clonogenic in transplantation analyses[51,52]. These observations have led to the fragmentation model as an alternative to the A_s. This proposes that syncytial stability can degrade causing a reversion of A_{al} to a more primitive identity[53].

To date, the ultimate test of stemness within spermatogonia has been by the injection of isolates into germline depleted testes[46,54]. Chemotherapies, such as busulfan treatment, can render a testis devoid of its highly mitotic germline. To similar effect, c-Kit mutations prevent proper migration of primordial germ cells to the gonadal ridge, during development and result in sterile, germline devoid testes[20,55–58]. Using treated or mutant mice, it was discovered that the subpopulations of A_{undiff} exhibit a variable capacity to colonize and establish spermatogenesis. The hierarchical model has been proposed based on this preferential ability of certain A_{undiff} populations to colonize germline devoid testes. This model defines an ultimate SSC, which gives rise to transient SSCs that maintain spermatogenesis, but are eventually lost to differentiation[49,59]. It is due to both the heterogeneity and interconvertibility of the A_{undiff} population that the absolute identification of an SSC and its niche has yet to occur.

1.3 Spermatogenesis in the fruit fly:

1.3.1 Testicular morphology

While ambiguity remains in the mammalian system, *Drosophila* provides a clear stromal niche for study. The fly testis consists of a coiled tubular structure, with sperm production occurring in a linear fashion along an apical to basal axis. The apical tip of the testis houses a grouping of somatic cells known as the hub. Attached to this structure are germline stem cells (GSCs) and cyst stem cells (CSCs), collectively forming a niche. With each division of a GSC, a new stem cell is produced, remaining attached to the hub, and a gonialblast results from the displaced daughter. Associated with the gonialblast are two CSC daughter cyst cells. The cyst cells extend cytoplasm to completely enclose the associated germline and all together form a structure known as a cyst. The enclosed gonialblast progresses through four mitotic amplifications resulting in 2,4,8, and 16 spermatogonia. Mitotic activity arrests and the now primary spermatocytes prepare for meiotic division. After a shuffling and halving of DNA content completing meiosis I, the secondary spermatocytes will again divide, in meiosis II, forming haploid cells. These spermatids under spermiogenesis, in which they elongate and produce a flagellum, thus forming spermatozoa. This schema maximally produces 64 sperm with every division of a GSC[60].

1.3.2 GSC Niche Signaling

With direct contact to a somatic structure, GSCs and CSC maintain this association via unpaired secretion from hub cells. This signaling acts via the Janus kinase-signal transducer and activator of transcription (JAK-STAT)

pathway to promote E-cadherin dependent adhesion in GSCs[61,62]. Both the hub and CSC provide local bone morphogenetic protein (BMP) signaling via ligands *decapentaplegic* and *glass bottom boat* to maintain GSCs in an undifferentiated state[63,64].

Unlike the mammalian SSC, little headway has been made in the *in vitro* culture of the GSC[65]. As such, less is known in regard to mitogenic factors similar to GDNF/FGF in the mouse. Insulin signaling is known to play a role, with starvation leading to a reduction in GSC population and proliferation[66]. Epidermal growth factor receptor ligand *spitz*/*stet* has also been demonstrated to regulate GSC mitotic activity in adult flies[67].

1.3.3 Conserved cellular characteristics

Remarkably, much of the hallmarks of sperm production are shared across metazoan taxa. Present in both invertebrates and mammals are cytoplasmic bridges between the expanding germline clones[68]. This allows for the timing of mitotic and meiotic divisions amongst a developmentally identical population. Germline has shown the need for somatic support in both systems[2]. The *Drosophila* cyst cells encompass and provide a conducive signaling environment, similar to the mouse Sertoli cell.

Both systems have also lent insights to the other, in regard to molecular features. VASA, a maternally inherited specifier of germline in the fly, has been shown to be present across the taxa, existing as mouse vasa homolog[69,70]. Similarly, NANOS, a marker or early stage germline in the fly, has two forms expressed in the mouse A_{undiff}, NANOS2 and NANOS3[71–74]. The role of NOTCH

was discovered in the mouse, serving as a mediator of differentiation in the adult, and maintaining quiescence in the prepuberal gonocyte[75–77]. Recent work in our lab has shown a similar role for notch in *Drosophila*, showing that germline survival is dependent on cyst cell-spermatogonia signaling[78]. While the mouse and fly testis are structurally divergent, it is clear there is insight to be shared between these systems.

References

1. Moller, A. P. Ejaculate Quality, Testes Size and Sperm Production in Mammals. *Funct. Ecol.* **3**, 91–96 (1989).
2. White-Cooper, H. & Bausek, N. Evolution and spermatogenesis. doi:10.1098/rstb.2009.0323.
3. Fayomi, A. P. & Orwig, K. E. Spermatogonial stem cells and spermatogenesis in mice, monkeys and men. *Stem Cell Res.* **29**, 207–214 (2018).
4. Nakata, H. *et al.* Three-dimensional structure of seminiferous tubules in the adult mouse. *J. Anat.* **227**, 686–94 (2015).
5. Phillips, B. T., Gassei, K. & Orwig, K. E. Spermatogonial stem cell regulation and spermatogenesis. *Philos. Trans. R. Soc. B Biol. Sci.* **365**, 1663–1678 (2010).
6. Griswold, M. D. Spermatogenesis: The Commitment to Meiosis. *Physiol. Rev.* **96**, 1–17 (2016).
7. Nakata, H. Morphology of mouse seminiferous tubules. *Anat. Sci. Int.* **94**, 1–10 (2019).
8. Bellvé, A. R. *et al.* Spermatogenic cells of the prepuberal mouse. Isolation and morphological characterization. *J. Cell Biol.* **74**, 68–85 (1977).
9. Clermont, Y. Kinetics of spermatogenesis in mammals: seminiferous epithelium cycle and spermatogonial renewal. *Physiological reviews* vol. 52 198–236 (1972).
10. LEBLOND, C. P. & CLERMONT, Y. Definition of the stages of the cycle of

the seminiferous epithelium in the rat. *Ann. N. Y. Acad. Sci.* **55**, 548–573 (1952).

11. OAKBERG, E. F. A description of spermiogenesis in the mouse and its use in analysis of the cycle of the seminiferous epithelium and germ cell renewal. *Am. J. Anat.* **99**, 391–413 (1956).
12. Tegelenbosch, R. A. & de Rooij, D. G. A quantitative study of spermatogonial multiplication and stem cell renewal in the C3H/101 F1 hybrid mouse. *Mutat. Res.* **290**, 193–200 (1993).
13. Monesi, V. Autoradiographic Study of DNA Synthesis and The Cell Cycle in Spermatogonia and Spermatocytes of Mouse Testis Using Tritiated Thymidine. *J. Cell Biol.* 1–18 (1962) doi:10.1083/jcb.14.1.1.
14. Hogarth, C. A. & Griswold, M. D. The key role of vitamin A in spermatogenesis. *J. Clin. Invest.* **120**, 956–62 (2010).
15. Mitranond, V., Sobhon, P., Tosukhowong, P. & Chindaduangrat, W. Cytological changes in the testes of vitamin-A-deficient rats. I. Quantitation of germinal cells in the seminiferous tubules. *Acta Anat. (Basel).* **103**, 159–68 (1979).
16. van Pelt, A. M. M. & de Rooij, D. G. Synchronization of the Seminiferous Epithelium after Vitamin A Replacement in Vitamin A-Deficient Mice. *Biol. Reprod.* **43**, 363–367 (1990).
17. Yoshida, S., Sukeno, M. & Nabeshima, Y. -i. A Vasculature-Associated Niche for Undifferentiated Spermatogonia in the Mouse Testis. *Science (80-.).* **317**, 1722–1726 (2007).

18. Shaha, C., Tripathi, R. & Mishra, D. P. Male germ cell apoptosis: regulation and biology. *Philsophical Trans. R. Soc. B.* **365**, 1501–1515 (2010).

19. Bendel-Stenzel, M., Anderson, R., Heasman, J. & Wylie, C. The origin and migration of primordial germ cells in the mouse. *Semin. Cell Dev. Biol.* **9**, 393–400 (1998).

20. Manova, K., Nocka, K., Besmer, P. & Bachvarova, R. F. Gonadal expression of c-kit encoded at the W locus of the mouse. *Development* **110**, 1057–69 (1990).

21. Dann, C. T. *et al.* Spermatogonial Stem Cell Self-Renewal Requires OCT4, a Factor Downregulated During Retinoic Acid-Induced Differentiation. *Stem Cells* **26**, 2928–2937 (2008).

22. Pesce, M., Wang, X., Wolgemuth, D. J. & Schöler, H. R. Differential expression of the Oct-4 transcription factor during mouse germ cell differentiation. *Mech. Dev.* **71**, 89–98 (1998).

23. Costoya, J. A. *et al.* Essential role of Plzf in maintenance of spermatogonial stem cells. *Nat. Genet.* **36**, 653–659 (2004).

24. Buaas, F. W. *et al.* Plzf is required in adult male germ cells for stem cell self-renewal. *Nat. Genet.* **36**, 647–652 (2004).

25. Lovelace, D. L. *et al.* The regulatory repertoire of PLZF and SALL4 in undifferentiated spermatogonia. *Development* **143**, 1893–1906 (2016).

26. Hobbs, R. M. *et al.* Functional Antagonism between Sall4 and Plzf Defines Germline Progenitors. *Cell Stem Cell* **10**, 284–298 (2012).

27. Gassei, K. & Orwig, K. E. SALL4 expression in gonocytes and

spermatogonial clones of postnatal mouse testes. *PLoS One* **8**, e53976 (2013).

28. van Bragt, M. P. A. *et al.* Expression of the pluripotency marker UTF1 is restricted to a subpopulation of early A spermatogonia in rat testis. *Reproduction* **136**, 33–40 (2008).
29. Yoshida, S. *et al.* Neurogenin3 delineates the earliest stages of spermatogenesis in the mouse testis. *Dev. Biol.* **269**, 447–458 (2004).
30. Zheng, K., Wu, X., Kaestner, K. H. & Wang, P. J. The pluripotency factor LIN28 marks undifferentiated spermatogonia in mouse. *BMC Dev. Biol.* **9**, 38 (2009).
31. Meng, X. *et al.* Regulation of cell fate decision of undifferentiated spermatogonia by GDNF. *Science* **287**, 1489–93 (2000).
32. Grasso, M. *et al.* Distribution of GFRA1-expressing spermatogonia in adult mouse testis. *Reproduction* **143**, 325–32 (2012).
33. Garbuzov, A. *et al.* Purification of GFRα1+ and GFRα1– Spermatogonial Stem Cells Reveals a Niche-Dependent Mechanism for Fate Determination. *Stem Cell Reports* **10**, (2018).
34. Sablitzky, F. *et al.* Stage- and subcellular-specific expression of Id proteins in male germ and Sertoli cells implicates distinctive regulatory roles for Id proteins during meiosis, spermatogenesis, and Sertoli cell function. *Cell Growth Differ.* **9**, 1015–24 (1998).
35. Chan, F. *et al.* Functional and molecular features of the Id4+ germline stem cell population in mouse testes. *Genes Dev.* **28**, 1351–1362 (2014).

36. Sun, F., Xu, Q., Zhao, D. & Degui Chen, C. Id4 Marks Spermatogonial Stem Cells in the Mouse Testis. *Sci. Rep.* **5**, 17594 (2015).

37. Aloisio, G. M. *et al.* PAX7 expression defines germline stem cells in the adult testis. *J. Clin. Invest.* **124**, 3929–3944 (2014).

38. Patel, H. & Bhartiya, D. Testicular Stem Cells Express Follicle-Stimulating Hormone Receptors and Are Directly Modulated by FSH. *Reprod. Sci.* **23**, 1493–1508 (2016).

39. Soffientini, U. *et al.* Identification of Sertoli cell-specific transcripts in the mouse testis and the role of FSH and androgen in the control of Sertoli cell activity. *BMC Genomics* **18**, (2017).

40. Takeda, H., Chodak, G., Mutchnik, S., Nakamoto, T. & Chang, C. Immunohistochemical localization of androgen receptors with mono- and polyclonal antibodies to androgen receptor. *J. Endocrinol.* **126**, 17–25 (1990).

41. Wang, J. *et al.* Androgen promotes differentiation of PLZF+ spermatogonia pool via indirect regulatory pattern. *Cell Commun. Signal.* **17**, (2019).

42. Shinohara, T., Avarbock, M. R. & Brinster, R. L. β1- and α6-integrin are surface markers on mouse spermatogonial stem cells. *Proc. Natl. Acad. Sci. U. S. A.* **96**, 5504–5509 (1999).

43. Kubota, H., Avarbock, M. R. & Brinster, R. L. Spermatogonial stem cells share some, but not all, phenotypic and functional characteristics with other stem cells. *PNAS* **100**, 6487–6492 (2003).

44. Oatley, J. M., Avarbock, M. R. & Brinster, R. L. Glial Cell Line-derived

Neurotrophic Factor Regulation of Genes Essential for Self-renewal of Mouse Spermatogonial Stem Cells Is Dependent on Src Family Kinase Signaling. *J. Biol. Chem.* **282**, 25842–25851 (2007).

45. Uchida, A. *et al.* In vivo dynamics of GFRα1-positive spermatogonia stimulated by GDNF signals using a bead transplantation assay. *Biochem. Biophys. Res. Commun.* **476**, 546–552 (2016).
46. Takashima, S. & Shinohara, T. Culture and transplantation of spermatogonial stem cells. *Stem Cell Res.* **29**, (2018).
47. Kubota, H. & Brinster, R. L. Culture of rodent spermatogonial stem cells, male germline stem cells of the postnatal animal. *Methods Cell Biol.* **86**, 59–84 (2008).
48. Oakberg, E. F. Spermatogonial stem-cell renewal in the mouse. *Anat. Rec.* **169**, 515–531 (1971).
49. de Rooij, D. G. The nature and dynamics of spermatogonial stem cells. *Development* **144**, 3022–3030 (2017).
50. Hara, K. *et al.* Mouse Spermatogenic Stem Cells Continually Interconvert between Equipotent Singly Isolated and Syncytial States. *Cell Stem Cell* **14**, 658–672 (2014).
51. Nakagawa, T., Sharma, M., Nabeshima, Y. i., Braun, R. E. & Yoshida, S. Functional Hierarchy and Reversibility Within the Murine Spermatogenic Stem Cell Compartment. *Science (80-.).* **328**, 62–67 (2010).
52. Nakagawa, T., Nabeshima, Y. & Yoshida, S. Functional Identification of the Actual and Potential Stem Cell Compartments in Mouse Spermatogenesis.

Dev. Cell **12**, 195–206 (2007).

53. Yoshida, S. Elucidating the identity and behavior of spermatogenic stem cells in the mouse testis. *Reproduction* **144**, 293–302 (2012).

54. Ogawa, T., Aréchaga, J. M., Avarbock, M. R. & Brinster, R. L. Transplantation of testis germinal cells into mouse seminiferous tubules. *Int. J. Dev. Biol.* **41**, 111–122 (1997).

55. Rossi, P., Sette, C., Dolci, S. & Geremia, R. Role of c-kit in mammalian spermatogenesis. *Journal of Endocrinological Investigation* vol. 23 609–615 (2000).

56. Gu, Y., Runyan, C., Shoemaker, A., Surani, A. & Wylie, C. Steel factor controls primordial germ cell survival and motility from the time of their specification in the allantois, and provides a continuous niche throughout their migration. *Development* **136**, 1295–1303 (2009).

57. Pesce, M., Di Carlo, A. & De Felici, M. The c-kit receptor is involved in the adhesion of mouse primordial germ cells to somatic cells in culture. *Mech. Dev.* **68**, 37–44 (1997).

58. Mauduit, C., Hamamah, S. & Benahmed, M. *Stem cell factor/c-kit system in spermatogenesis*. *Human Reproduction Update* vol. 5 (1999).

59. Lord, T. & Oatley, J. M. A revised Asingle model to explain stem cell dynamics in the mouse male germline. *Reproduction* **154**, R55–R64 (2017).

60. Fuller, M. T. Spermatogenesis. in *The Development of Drosophila Melanogaster* (eds. Bate, M. & Martinez Arias, A.) 71–147 (Cold Spring

Harbor Laboratory Press, 1993).

61. Tulina, N. & Matunis, E. Control of stem cell self-renewal in Drosophila spermatogenesis by JAK-STAT signaling. *Science* **294**, 2546–9 (2001).

62. Leatherman, J. L. & Dinardo, S. Germline self-renewal requires cyst stem cells and stat regulates niche adhesion in Drosophila testes. *Nat. Cell Biol.* **12**, 806–11 (2010).

63. Schulz, C. *et al.* A misexpression screen reveals effects of bag-of-marbles and TGF beta class signaling on the Drosophila male germ-line stem cell lineage. *Genetics* **167**, 707–23 (2004).

64. Kawase, E., Wong, M. D., Ding, B. C. & Xie, T. Gbb/Bmp signaling is essential for maintaining germline stem cells and for repressing bam transcription in the Drosophila testis. *Development* **131**, 1365–1375 (2004).

65. Kawamoto, T., Kawai, K., Kodama, T., Yokokura, T. & Niki, Y. Autonomous differentiation of Drosophila spermatogonia in vitro. *Dev. Growth Differ.* **50**, 623–632 (2008).

66. McLeod, C. J., Wang, L., Wong, C. & Jones, D. L. Stem cell dynamics in response to nutrient availability. *Curr. Biol.* **20**, 2100–5 (2010).

67. Parrott, B. B., Hudson, A., Brady, R. & Schulz, C. Control of germline stem cell division frequency--a novel, developmentally regulated role for epidermal growth factor signaling. *PLoS One* **7**, e36460 (2012).

68. Greenbaum, M. P., Iwamori, T., Buchold, G. M. & Matzuk, M. M. Germ cell intercellular bridges. *Cold Spring Harb. Perspect. Biol.* **3**, a005850 (2011).

69. Raz, E. The function and regulation of vasa-like genes in germ-cell

development. *Genome biology* vol. 1 (2000).

70. Tanaka, S. S. *et al.* The mouse homolog of Drosophila Vasa is required for the development of male germ cells. *Genes Dev.* **14**, 841–853 (2000).
71. Asaoka, M., Sano, H., Obara, Y. & Kobayashi, S. Maternal nanos regulates zygotic gene expression in germline progenitors of Drosophila melanogaster. *Mech. Dev.* **78**, 153–158 (1998).
72. Tsuda, M. *et al.* Conserved role of nanos proteins in germ cell development. *Science* **301**, 1239–41 (2003).
73. Suzuki, A., Tsuda, M. & Saga, Y. Functional redundancy among Nanos proteins and a distinct role of Nanos2 during male germ cell development. *Development* **134**, 77–83 (2007).
74. Sada, A., Hasegawa, K., Pin, P. H. & Saga, Y. NANOS2 Acts Downstream of Glial Cell Line-Derived Neurotrophic Factor Signaling to Suppress Differentiation of Spermatogonial Stem Cells. *Stem Cells* **30**, 280–291 (2012).
75. Dirami, G., Ravindranath, N., Achi, M. V. & Dym, M. Expression of Notch pathway components in spermatogonia and sertoli cells of neonatal mice. *J. Androl.* **22**, 944–952 (2001).
76. Garcia, T. X., DeFalco, T., Capel, B. & Hofmann, M. C. Constitutive activation of NOTCH1 signaling in Sertoli cells causes gonocyte exit from quiescence. *Dev. Biol.* **377**, 188–201 (2013).
77. Xavier Garcia, T. & Hofmann, M.-C. NOTCH signaling in Sertoli cells regulates gonocyte fate. *Cell Cycle* **12**, 2538–2545 (2013).

78. Ng, C. L., Qian, Y. & Schulz, C. Notch and Delta are required for survival of the germline stem cell lineage in testes of Drosophila melanogaster. *PLoS One* **14**, e0222471 (2019).

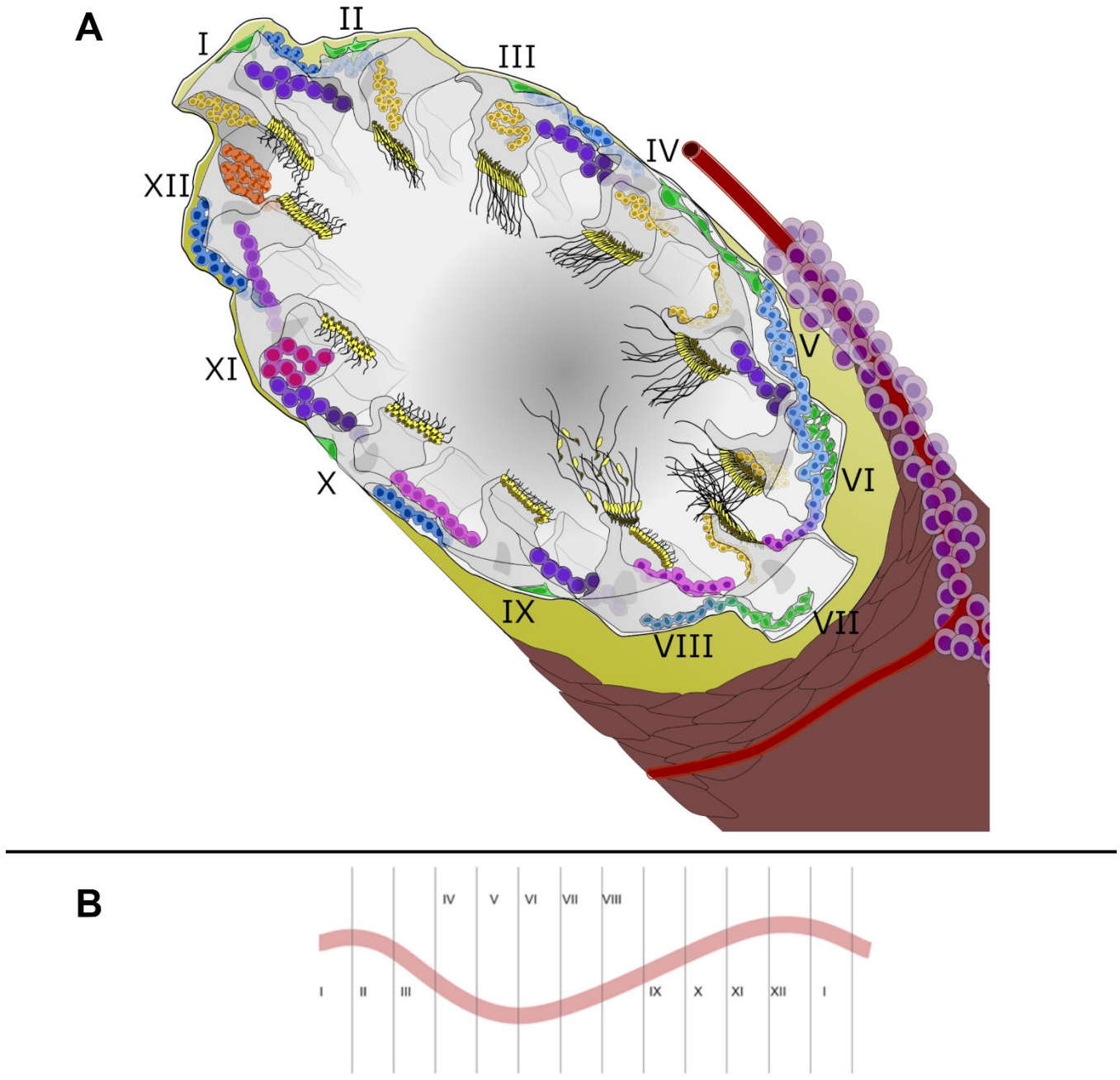

Figure 1.1 Progression and staging of spermatogenesis

A) A cartoon depiction of the murine testis tubule and the stages of the seminiferous cycle. Interstitium (purple), vasculature (red line) and basement membrane (yellow). Sertoli cells (gray), A_{undiff} (green), $A_{1\text{-}4}$ (teal, blue), primary

spermatocytes (purple), secondary spermatocytes (orange), round and elongating spermatids (yellow). Stages indicated by roman numeral (I-XII). B) Longitudinal ordering of spermatogenic cycle stages.

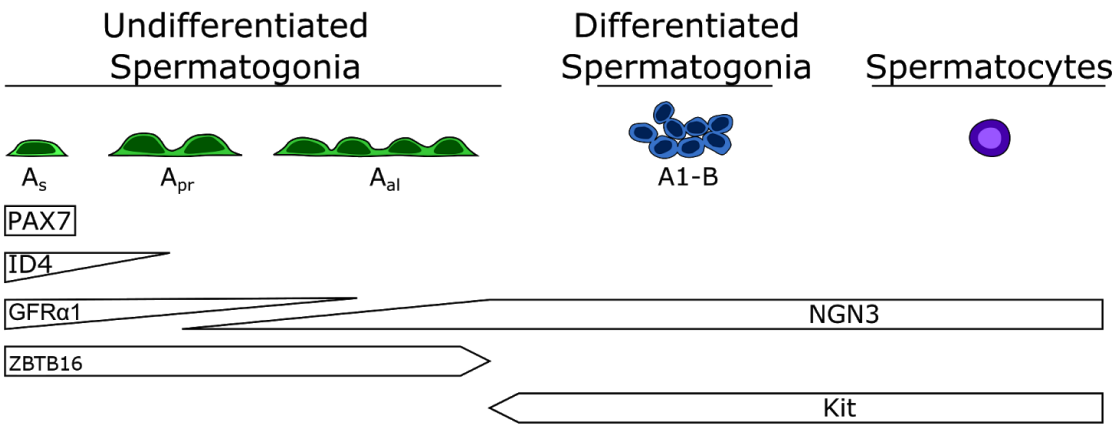

Figure 1.2 Heterogeneity amongst mammalian spermatogonial markers

Distribution of cell type and syncytial state using various molecular markers.

Undifferentiated Type A spermatogonia single (A_s), paired (A_{pr}), and aligned (A_l).

CHAPTER 2

Shining a thin light on the testis: application of light-sheet fluorescence microscopy in the mouse male gonad

Karl A. Kudyba, James D. Lauderdale, and Cordula Schulz. 2019. *To be submitted to Scientific Reports*

Abstract

The mammalian testis has a challenging architecture, containing winding tubules in which germline cells differentiate in a spatio-temporal pattern across multiple axes. In part this challenging structure has obscured the absolute identification of a germline stem cell. Previous approaches to study the testes structure and the cells inside of it have come at significant time cost or result in loss of tissue arrangement. Here we employ tissue clearing and light-sheet microscopy in the mouse testis. We utilize computer aided stereology as a means to examine label efficacy with multiple relevant stem cell markers. Doing so allows for a new look at cell-type distribution in the winding tubule structure.

Introduction

Adult stem cells replenish specialized cells of many tissues throughout the lifetime of an organism. Constant tissue turnover is possible due to a stem cells ability to self-renew and to produce differentiating daughter cells. However, the study of these cells presents a considerable challenge because of their rarity, being outnumbered by their parenchymal daughters[1]. Further hindering their study, are the complicated architectures produced by the tissues they replenish. The convoluted tubules of the mammalian testis provide such a challenge, where the identity of an absolute spermatogonial stem cell (SSC) remains a debate[2–4]. Histological sectioning and staining have long provided insights into this elusive population; however, these techniques reduce tissue complexity to XY dimensionality. The benefits of three-dimensional reconstruction are clear, yet this remains a seldom used process in the testis due to technical challenges and

labor intensity. Light-sheet fluorescence microscopy (LSFM) represents a significant advance in this regard.

The mammalian testis houses a network of winding tubules that contain developing germline cells distributed between somatic Sertoli cells. An interstitial compartment, between the tubules, is populated by capillaries, macrophages, and hormone producing Leydig cells. Along with Sertoli cells, the interstitium contributes to a niche conducive for SSC maintenance[5,6]. The germline has been broadly classified into mitotically active spermatogonia, meiotic spermatocytes, haploid spermatids, and the morphologically remodeled spermatozoa[7–9] (Figure 2.1A). Spermatogonia, determined to be the most primitive of the spermatogenic lineage, are distributed along the peripheral basement membrane while all other germline cells are located away from the membrane and towards the lumen. The spermatogonia are further subdivided into three types based stained nuclear profile (A, Intermediate (In), and B). Among the type A is an undifferentiated subpopulation, A_{undiff}, which are the precursor cells that give rise to all later stages of germline. The SSCs reside amongst this group and are thought to represent 0.03% of the germline [10,11].

In the rodent, high mitotic activity of spermatogonia, along with the progression of their lineages through differentiation, gives rise to a wave-like arrangement of the developing germline cells through a tubules length[12]. As a result, while differentiation occurs in a marginal to luminal fashion, individual cross-sections will only demonstrate a partial sample of the cell-types. This architecture necessitates a 3D approach to examine the entire seminiferous

cycle within a single tubule. Previous studies have tackled this problem through serial sections or dissociating the tissue into linearized tubule whole mounts, the former being labor and time intensive, while the latter destroys the relationship to interstitial cells[6,13,14].

With the pursuit of an SSC and its potential niche involving small populations relative to the entire tissue, LSFM stands out as a powerful untapped tool. By focusing a laser into a singular plane of illumination, optical sections can be rapidly acquired in translucent tissues[15]. These microscopes vary in design and can be straightforward to build, operate, and maintain[16]. Recent advances in tissue clearing techniques have allowed for intact opaque samples to be rendered optically translucent through delipidating and immersing in a medium with sufficiently low optical density[17]. Pairing the two techniques potentiates a rapid approach to three-dimensional histologic analyses. Despite the great potential, its uses in adult tissues have largely been restricted to neurological studies.

Here we utilize the immunolabeling-enabled three-dimensional imaging of solvent-cleared organs (iDISCO) clearing procedure to render testes visibly translucent, allowing for use of LSFM[18]. We demonstrate the efficacy of signal penetrance into deep tissue by automated quantification of the A_{undiff} population at various tissue depths. Furthermore, we investigate the potential of this approach in analysis of structural features such as tissue staging and interstitial relationship. Lastly, we examine the ability to image putative SSC populations.

Materials and Methods

Mice

C57BL/6 mice were obtained from Jackson Laboratory. LT-11 mice carrying an ID4-egfp reporter were shared from Oatley lab and maintained as a heterozygous population in C57BL/6 background. All mice were housed in standard conditions and allowed unrestricted access to sustenance. Primary euthanization was conducted via either lethal dose of Avertin or carbon dioxide asphyxiation, followed by secondary means of pneumothoracic perforation. All mice were maintained, and experiments conducted, with permission of the University of Georgia's Institutional Animal Care and Use Committee.

Tissue Processing and staining

Immediately following euthanization adult mice were perfused with two volumes of phosphate- buffered saline (PBS) then 4% paraformaldehyde (PFA)/PBS. Testes were harvested *en grosse* and maintained on ice until the tunica albuginea was removed and then transferred to 4% PFA/PBS overnight at 4C. The fixed tissue was washed in PBS, serially dehydrated with methanol, and subsequently stored at -20C in 100% methanol until utilized.

Following fixation and storage, the tissue was processed per iDISCO protocol summarized as follows[18]. Testes were treated to overnight delipidating in 2:1 dichloromethane(DCM)/ methanol at room temperature, followed by methanol washes, and then bleached in 5% Hydrogen peroxide/methanol overnight at 4C. Serial rehydration and washes were performed, after which the testes were further washed in 0.2% PBS-TritonX-100(Ptx.2). Permeabilization continued at

37C in Ptx.2 with the addition of 20% dimethyl sulfoxide (DMSO) and glycine at 23 g/L. Tissue was blocked at 37C in Ptx.2, 10% DMSO and 6% donkey serum (DKS), and followed by incubation with primary antibody in 0.2% PBS-Tween20 with 10ug/mL Heparin (PTwH), supplemented with 5%DMSO and 3% DKS continued at the same temperature. Excess primary was washed out in successive PTwH washes. Secondary labeling was conducted at 37C in PTwH with 3% DKS. Secondary antibody was washed out in PTwH and samples were held in PTwH overnight at 4C. To aid in tissue handling, testes were embedded in 1% agarose in PBS before subsequent serial dehydration in methanol. Final delipidating began with 2:1 DCM/methanol with the testes being transferred to two incubations in 100% DCM after sinking. The labeled tissues are finally stored in dibenzyl ether at room temperature until imaging.

Primary antibodies used in this study were rabbit anti-plzf (Santa Cruz H-300), goat anti-hplzf (R&D Systems, AF2944), goat anti-gfrα1 (R&D Systems, AF560), chicken anti-GFP (Aves GFP-1010). Secondary antibodies used were Alexa Fluor 790 donkey anti-rabbit (Invitrogen A11374), Alexa Fluor 594 donkey anti-rabbit (Invitrogen A32754), Alexa Fluor 594 donkey anti-goat (Invitrogen A32758), Alexa Fluor 647 donkey anti-chicken (Jackson ImmunoResearch AB_2340379).

Image Acqusition

Imaging was conducted in DBE at 2-3um optical slice increments on a LaVision Biotec Ultrascope II fitted with Olympus MVX-10 Zoom Body and Olympus MVPLAPO 2x Objective (NA 0.5). Sheet NA was set between 6-8um

and width was 100%- 30% dependent on zoom factor (6.4x or 12.6x). Images were captured using either bidirectional sheets or single side illumination at a 16-bit depth and 20ms exposure.

Image Analysis

Image were analyzed in Imaris 9.5. For the signal penetrance assay, 432um x 432um x 900um volumes were cropped from image stacks through the minor axis of a testis. ZBTB16^{+} cells were identified using the provided spot algorithm. Mean intensities were measured within the 10.7 um diameter spot volumes and normalized per testis. Tubules were outlined as Imaris surface contours using fluorescent background for boundary discernment. Interstitial regions appear brightly under 488nm laser illumination and were identified by simple threshold.

In order to determine cell density along the longitudinal axis, a distance map was made for binary masked tubule regions. A filament object was created based on intensity of the created map. Central axis vertices were exported along with the spot location and intensity information. Using numpy module in Python 3.7, spot positions were related to the nearest vertex and a threshold applied into bright or dim groups. A histogram and kernel density estimate was used to plot the cell population probabilities along the tubule axis. All graphs generated in Python using matplotlib and seaborn modules.

Results

iDisco/LSFM labels and penetrates into deep tissue.

In large tissues, LSFM can face a twofold challenge of signal penetrance. First, the tissue must be adequately permeabilized for antibody labeling, without destroying superficial signal. Secondly, intense fluorescence on the tissue margin can hinder or completely prevent deep signal acquisition, requiring labeling to be sparse. Also, achieving full clarification of the tissue is equally important to prevent image distortion. In addition to the above challenges, the murine testis is surrounded by the tunica albuginea that provides a substantial barrier to penetrance, and often becomes brightly marked during immunolabeling (data not shown). For this reason, it was removed in all experiments.

Spermatogonia are heterogeneous and can be delineated by a vast and growing array of markers. The A_{undiff} population can easily be visualized with antibodies against Zinc finger and BTB domain containing 16 (ZBTB16), a transcriptional repressor necessary for the maintenance of the undifferentiated state within A_{undiff}[19]. Anti-ZBTB16 is a robust antibody that labels A_{undiff} brightly and differentiating $A_{1\text{-}3}$ dimly [6]. Thus, we employed this well-established antibody for labeling and imaged z-stacks through a region of the tubule. To test antibody penetrance, we focused on a central region of the testis short axis (medial-lateral or dorsal-ventral). Our optical sections in this area showed a similar patterning compared to histological sections (Figure 2.1B, B'). Bright and dim ZBTB16 staining was observed in a subset of spermatogonia along the tubule margin (Figure 2.1B', arrowheads). Differential staining was also apparent in Z-stack

projections (Figure 2.1C) and the Imaris spot-finding algorithm identified individual ZBTB16-positive cells (Figure 2.1C'). As a measure for showing tissue penetrance and for quantification of the signal we analyzed captured Z-stacks of identically sized regions from the top, middle, and bottom of the tubule section and applied a spot-finding algorithm to identify individual cells. Based on the normalized intensities, it appeared that the superficial top and bottom regions had somewhat brighter overall signal than the deeper regions (Figure 2.1D), likely due to increased absorbance in larger sections of the tissue. However, A_{undiff} were equally identifiable across all three regions (Figure 2.1D), showing that the antibody penetrated all areas of the testes in our procedure.

LSFM allowed for observation of tissue state and arrangement

By masking image stacks, we have the ability to conduct samplings of individual tubules. This effectively gives the view of a whole mount approach within intact tissue (Figure 2.2A). ZBTB16 labeled cell abundance has been reported in terms of tubule cross-section, surface area, and per 1000 Sertoli cells[5,6,11]. While we did not test markers for Sertoli cells, we related the cell populations to masked tubule surface area. Across 3 mice and we found an average of 32.6 $ZBTB16^{+}$ per $10^{5}\,mm^{2}$ with a standard deviation of 6.2.

We next asked if the variable state of seminiferous cycle could be readily observed. The mouse tubule can be segmented into 12 stages (I-XII), originally characterized by histological appearance of acrosomal development[12]. ZBTB16 population dynamics have been shown to be reflective of this cycle and can be used to broadly stage tubules. The brightly marked A_{undiff} population is most

abundant during stages I to VI, increasing in density throughout the length of these regions. Stage VII to VIII marks a transition at which point differentiation is induced by a pulse of retinoic acid. This manifests in stage VIII to XII being populated by mostly dimly marked $A_{1\text{-}3}$, with low numbers of A_{undiff}[6,20]. Such a populational shift could be observed in masked tubules. By relating fluorescent intensity of cells along the central tubule axis (red line in Figure 2.2A') we are able to distinguish tubule progression through the seminiferous cycle. Within the sampled tubule, bright spermatogonia were detected consistently across 2.5mm, while dim spermatogonia were primarily detected from 2.75mm to 3.5mm along the axis (Figure 2.2B).

We next sought to utilize the imaging of intact tissue to relate A_{undiff} populations to the interstitial compartment. Previous analysis has shown that a subset of A_{undiff} are largely clustered along the interstitial-tubule border, based on labeling with another marker, Neuregulin 3 (NGN3)[5]. We took advantage of the interstitial fluorescence at 488nm (red in Figure 2.2C, C') to threshold and distinguish the region without hand labeling in testes labeled for anti-ZBTB16 (green in Figure 2.2C). Using 3-D reconstructions, we were able to measure the distance of the brightly labeled $ZBTB16^{+}$ A_{undiff} cells to the border of the interstitium. Cells within 30um of the interstitium were considered near (purple dots in Figure 2.2C'), while cells further away were classified as far (blue cells in Figure 2.2C'). Consistent with the previous observation using NGN3 populations, the majority of the A_{undiff} cells brightly labeled for ZBTB16 were found mostly adjacent to interstitial regions (Figure 2.2D).

Identification of potential SSCs with GFRα1 and ID4 using LSFM

To date a consensus characterization of the SSC has yet to be achieved, leading to two primary models of spermatogonial renewal, the fragmentation model and the hierarchical model, each with a population identifying label[2]. The A_{undiff} can be further characterized by the number of divisions and the cytoplasmic bridges that interconnect these early stage germline cells. A_s are isolated single cells that are not interconnected by bridges. A_{pr} result from an incomplete division of A_s, while A_{al} are increasing length chains of 4, 8, or 16 interconnected A_{undiff}[12]. GDNF family receptor alpha 1 (GFRα1) marks A_s up to A_{al4}, though it does not encompass the entirety of cells in these syncytial states. This population has been shown to remain fluid, expanding through to A_{al4} and stochastically collapsing cellular bridges to form the varying sets of A_s+A_{al3} or 2 A_{pr}. Deemed the fragmentation model, it is suggested that this stem cell population is dynamically maintained amongst a mobile and varying sized pool[21].

We used our technology to ask if we can detect cells expressing GFRα1 within our population of ZBTB16-positive cells. As expected, GFRα1 co-localized with bright ZBTB16+ cells (Figure 2.3A-B).[14] Cell density measurements along the axis confirmed that GFRα1 co-localized with brightly stained ZBTB16 cells (Figure 2.3C). However, as apparent in optical sections, GFRα1 only co-localized to a subset of the brightly stained ZBTB16 cells (Figure 2.3C, arrows).

Several recent markers, including inhibitor of DNA binding 4 (ID4), paired box 7 (PAX7), and B cell-specific Moloney murine leukemia virus integration site 1 (BMI1) have been shown to subdivide A_s cells and these cells are able to

repopulate germline depleted testes at high efficiencies[22–26]. The hierarchical model supposes that these rare A_s cells are “ultimate” stem cells and divide to regenerate a transient pool of stem-like daughters[4]. Using the LT-11, ID4-eGFP transgenic mouse we used an anti-GFP antibody, as endogenous fluorescence is quenched during the clearing process. Consistent with initial reporting of ID4 expression we detected GFP in late stage spermatocytes and spermatids (Figure 2.3, green signal). [27] Most importantly, we observed GFP-labeling in a subset of GFRα1$^+$/ZBTB16$^+$ cells (arrowhead in Figure 2.3C), indicative of stem cell identity. Our analysis shows that LSFM is a relatively quick and reliable technique to identify cells within murine testes that express SSC markers.

Discussion

Here we demonstrated the effectiveness of tissue clearing paired with LSFM within the adult mouse testis. We were able to identify the A_{undiff} population through labeling and thresholding based on ZBTB16 intensity. Tubule architecture was identified and used to extract seminiferous cycle information with a single label and background fluorescence. Furthermore, using computer recognition and analysis, cell populations were discerned and related to interstitial regions. Finally, we demonstrated the ability to label putative SSC populations.

Previous approaches in 3D analysis have required painstaking reconstructions of histological sections. After harvesting, the tissue is sliced, imaged, aligned, masked, and rendered, requiring a large amount of hands-on time. Using such an approach it was shown that the A_{undiff} population, marked by

GFP under Ngn3 regulatory elements, preferentially located to regions of the tubule neighboring interstitium[5]. More recently entire testes were reconstructed. Utilizing computer recognition of stained basement membrane to expedite post imaging analysis, the authors produced a complete mapping of the convoluted arrangement of tubules[28]. The use of tissue clearing/LSFM studies provides a useful tool for more rapid tubule discernment.

In regard to the search for SSC identity, several single cell sequencing projects have been conducted and exist as a database for putative markers[29–31]. iDISCO/LSFM could serve as a powerful investigative tool in our understanding of this elusive population. Our ability to easily detect SSCs with such markers should aid in their further characterization. With iDISCO/LSFM at hand, SSC variation within one and among different populations of animals can easily be monitored. Variations in SSC numbers or behavior under changing environmental conditions, as well as in mutant background can quickly be assessed and contribute to our understanding of the factors that regulate SSCs. Likewise, much of the testis architectural arrangement remains an open field to explore. Sertoli cells have been shown to modify expression based on stage[32]. Additionally, macrophages play an important, yet largely unstudied, roll in maintenance of A_{undiff}[6]. How these niche arrangements and variations affect the putative SSC populations remain to be seen.

Acknowledgements

The authors would like to acknowledge Jon Oatley for the LT-11 mice. Madison Grant for initial interest in LSFM and assistance in microscope procurement.

Muthugapatti Kandasamy at the University of Georgia Biomedical Microscopy Core for provided technical assistance. Heather Kudyba, Robert Ng, Manashree Malpe, and Ashley Rasys provided helpful discussion.

References:

1. Klein, A. M. & Simons, B. D. Universal patterns of stem cell fate in cycling adult tissues. *Development* **138**, 3103–11 (2011).
2. de Rooij, D. G. The nature and dynamics of spermatogonial stem cells. *Development* **144**, 3022–3030 (2017).
3. Yoshida, S. Elucidating the identity and behavior of spermatogenic stem cells in the mouse testis. *Reproduction* **144**, 293–302 (2012).
4. Lord, T. & Oatley, J. M. A revised Asingle model to explain stem cell dynamics in the mouse male germline. *Reproduction* **154**, R55–R64 (2017).
5. Yoshida, S., Sukeno, M. & Nabeshima, Y. -i. A Vasculature-Associated Niche for Undifferentiated Spermatogonia in the Mouse Testis. *Science (80-.).* **317**, 1722–1726 (2007).
6. DeFalco, T. *et al.* Macrophages Contribute to the Spermatogonial Niche in the Adult Testis. *Cell Rep.* **12**, 1107–1119 (2015).
7. Phillips, B. T., Gassei, K. & Orwig, K. E. Spermatogonial stem cell regulation and spermatogenesis. *Philos. Trans. R. Soc. B Biol. Sci.* **365**, 1663–1678 (2010).
8. Bellvé, A. R. *et al.* Spermatogenic cells of the prepuberal mouse. Isolation and morphological characterization. *J. Cell Biol.* **74**, 68–85 (1977).
9. Clermont, Y. Kinetics of spermatogenesis in mammals: seminiferous epithelium cycle and spermatogonial renewal. *Physiological reviews* vol. 52 198–236 (1972).

10. Oakberg, E. F. Spermatogonial stem-cell renewal in the mouse. *Anat. Rec.* **169**, 515–531 (1971).
11. Tegelenbosch, R. A. & de Rooij, D. G. A quantitative study of spermatogonial multiplication and stem cell renewal in the C3H/101 F1 hybrid mouse. *Mutat. Res.* **290**, 193–200 (1993).
12. OAKBERG, E. F. A description of spermiogenesis in the mouse and its use in analysis of the cycle of the seminiferous epithelium and germ cell renewal. *Am. J. Anat.* **99**, 391–413 (1956).
13. Nakata, H., Sonomura, T. & Iseki, S. Three-dimensional analysis of seminiferous tubules and spermatogenic waves in mice. *Reproduction* **154**, 569–579 (2017).
14. Grasso, M. *et al.* Distribution of GFRA1-expressing spermatogonia in adult mouse testis. *Reproduction* **143**, 325–32 (2012).
15. Power, R. M. & Huisken, J. A guide to light-sheet fluorescence microscopy for multiscale imaging. *Nat. Methods* **14**, 360–373 (2017).
16. Power, R. M. & Huisken, J. Adaptable, illumination patterning light sheet microscopy. *Sci. Rep.* **8**, (2018).
17. Ariel, P. A beginner's guide to tissue clearing. *International Journal of Biochemistry and Cell Biology* vol. 84 35–39 (2017).
18. Renier, N. *et al.* iDISCO: A Simple, Rapid Method to Immunolabel Large Tissue Samples for Volume Imaging. *Cell* **159**, 896–910 (2014).
19. Costoya, J. A. *et al.* Essential role of Plzf in maintenance of spermatogonial stem cells. *Nat. Genet.* **36**, 653–659 (2004).

20. Meistrich, M. L. & Hess, R. A. Assessment of spermatogenesis through staging of seminiferous tubules. *Methods Mol. Biol.* **927**, 299–307 (2013).

21. Hara, K. *et al.* Mouse Spermatogenic Stem Cells Continually Interconvert between Equipotent Singly Isolated and Syncytial States. *Cell Stem Cell* **14**, 658–672 (2014).

22. Chan, F. *et al.* Functional and molecular features of the Id4+ germline stem cell population in mouse testes. *Genes Dev.* **28**, 1351–1362 (2014).

23. Oatley, M. J., Kaucher, A. V., Racicot, K. E. & Oatley, J. M. Inhibitor of DNA Binding 4 Is Expressed Selectively by Single Spermatogonia in the Male Germline and Regulates the Self-Renewal of Spermatogonial Stem Cells in Mice1. *Biol. Reprod.* **85**, 347–356 (2011).

24. Sun, F., Xu, Q., Zhao, D. & Degui Chen, C. Id4 Marks Spermatogonial Stem Cells in the Mouse Testis. *Sci. Rep.* **5**, 17594 (2015).

25. Aloisio, G. M. *et al.* PAX7 expression defines germline stem cells in the adult testis. *J. Clin. Invest.* **124**, 3929–3944 (2014).

26. Komai, Y. *et al.* Bmi1 expression in long-term germ stem cells. *Sci. Rep.* **4**, 6175 (2014).

27. Sablitzky, F. *et al.* Stage- and subcellular-specific expression of Id proteins in male germ and Sertoli cells implicates distinctive regulatory roles for Id proteins during meiosis, spermatogenesis, and Sertoli cell function. *Cell Growth Differ.* **9**, 1015–24 (1998).

28. Nakata, H. *et al.* Three-dimensional structure of seminiferous tubules in the adult mouse. *J. Anat.* **227**, 686–94 (2015).

29. Green, C. D. *et al.* A Comprehensive Roadmap of Murine Spermatogenesis Defined by Single-Cell RNA-Seq Data Resources GSE112393 Green et al. *Dev. Cell* **46**, 651–667 (2018).

30. Lukassen, S., Bosch, E., Ekici, A. B. & Winterpacht, A. Characterization of germ cell differentiation in the male mouse through single-cell RNA sequencing OPEN. *Sci. Rep.* **8**, 6521 (2018).

31. Hermann, B. P. *et al.* The Mammalian Spermatogenesis Single-Cell Transcriptome, from Spermatogonial Stem Cells to Spermatids. *Cell Rep.* **25**, 1650-1667.e8 (2018).

32. Timmons, P. M., Rigby, P. W. J. & Poirier, F. The murine seminiferous epithelial cycle is pre-figured in the Sertoli cells of the embryonic testis. *Development* **129**, 635–647 (2002).

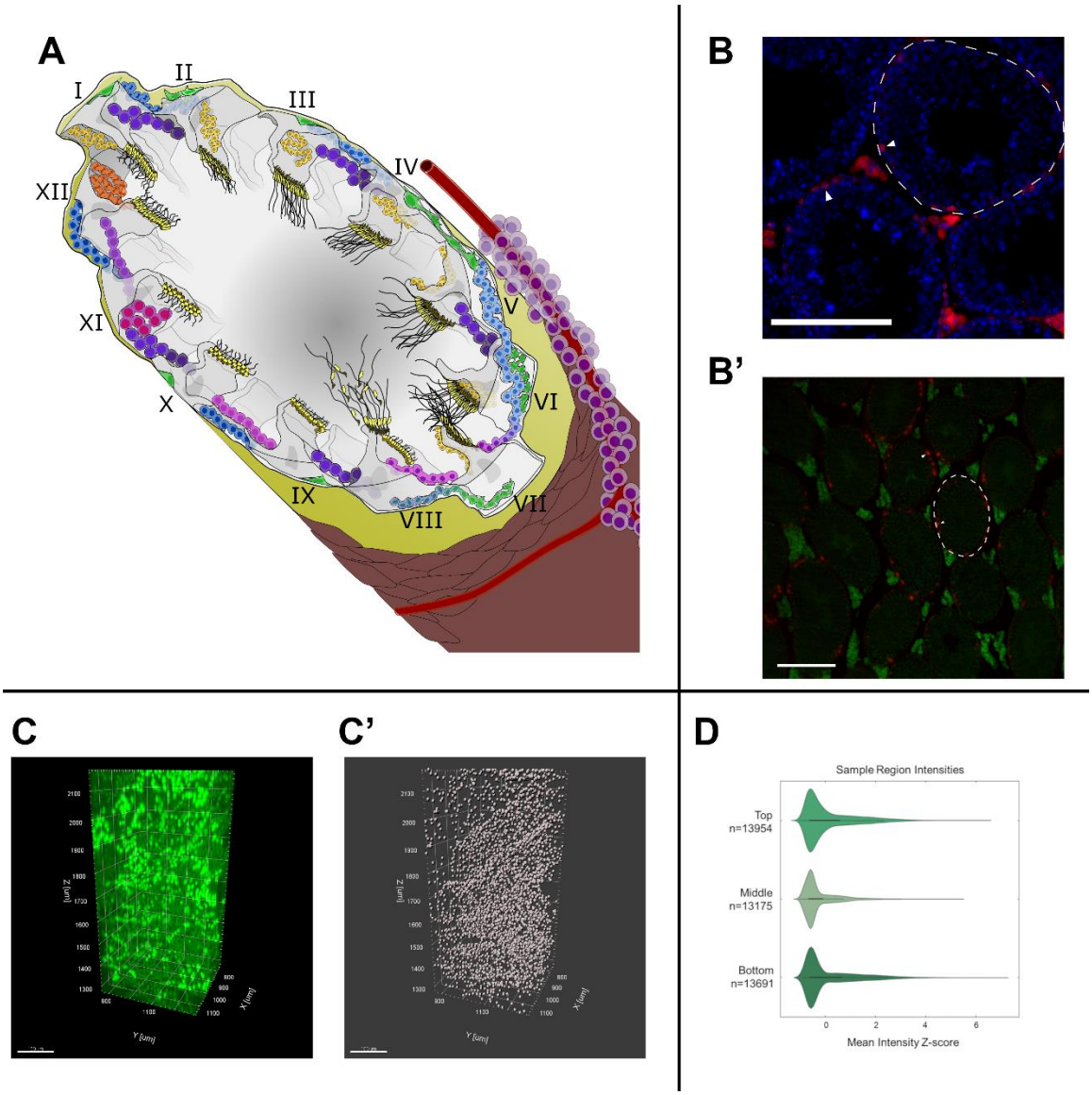

Figure 2.1 Antibody suitably penetrates testis tissue with iDISCO/LSFM

A) A cartoon depiction of the murine testis tubule and the stages of the seminiferous cycle. Interstitium (purple), vasculature (red line) and basement membrane (yellow). Sertoli cells (gray), A_{undiff} (green), $A_{1\text{-}4}$ (teal, blue), primary spermatocytes (purple), secondary spermatocytes (orange), round and elongating spermatids (yellow). Stages indicated by roman numeral (I-XII).

B, B') ZBTB16 stained (red) tissue in (B) histologic section (blue: DAPI, scalebar = 200μm); and (B') optical section (green: tissue background, scalebar = 200μm). White dashes outline a tubule, arrowhead: ZBTB16^{+} cells.

C) 3D projection of sampled region and C') Spot algorithm of ZBTB16 signal.

D) Regional assessment of normalized mean intensity values, as indicated (n=3 mice/6 testes).

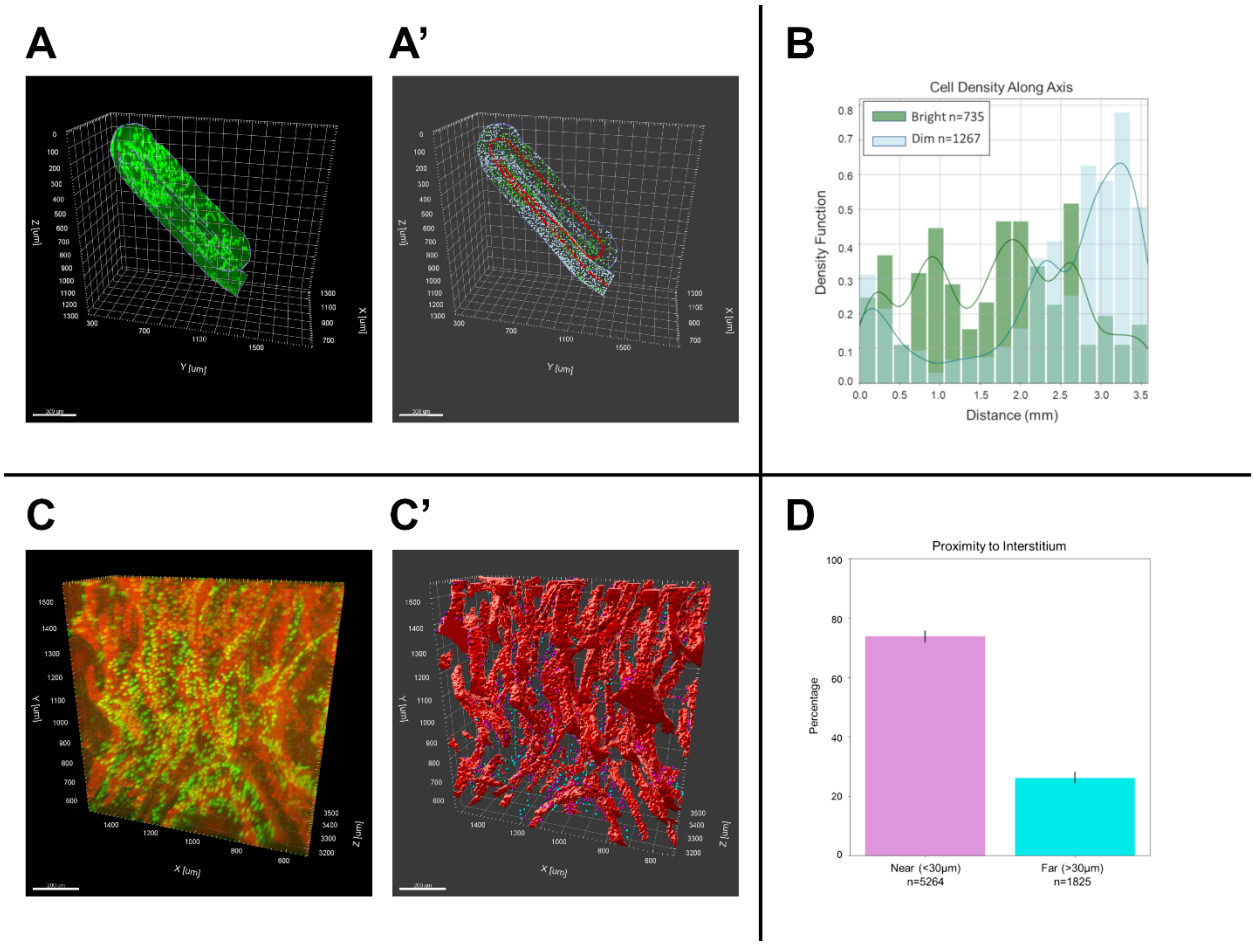

Figure 2.2. Figure 2. iDISCO/LSFM reveals structural features

A) 3D projection and (A’) spot identification (bright: green, dim: light blue) in a masked tubule (tubule: dark blue, axis: red).

B) Histogram and kernel density estimation of bright and dim ZBTB16 labeled cells in relation to the tubule axis. Green line represents distribution of bright cells, blue line represents distribution of dim cells.

C) 3D projection (ZBTB16 in green) and (C’) spot/surface identification of ZBTB16 bright cells (near: purple, far: cyan) and interstitial 488nm background (red).

D) Quantification of ZBTB16 bright cells in relation to interstitial regions (n=4 mice/4 testes).

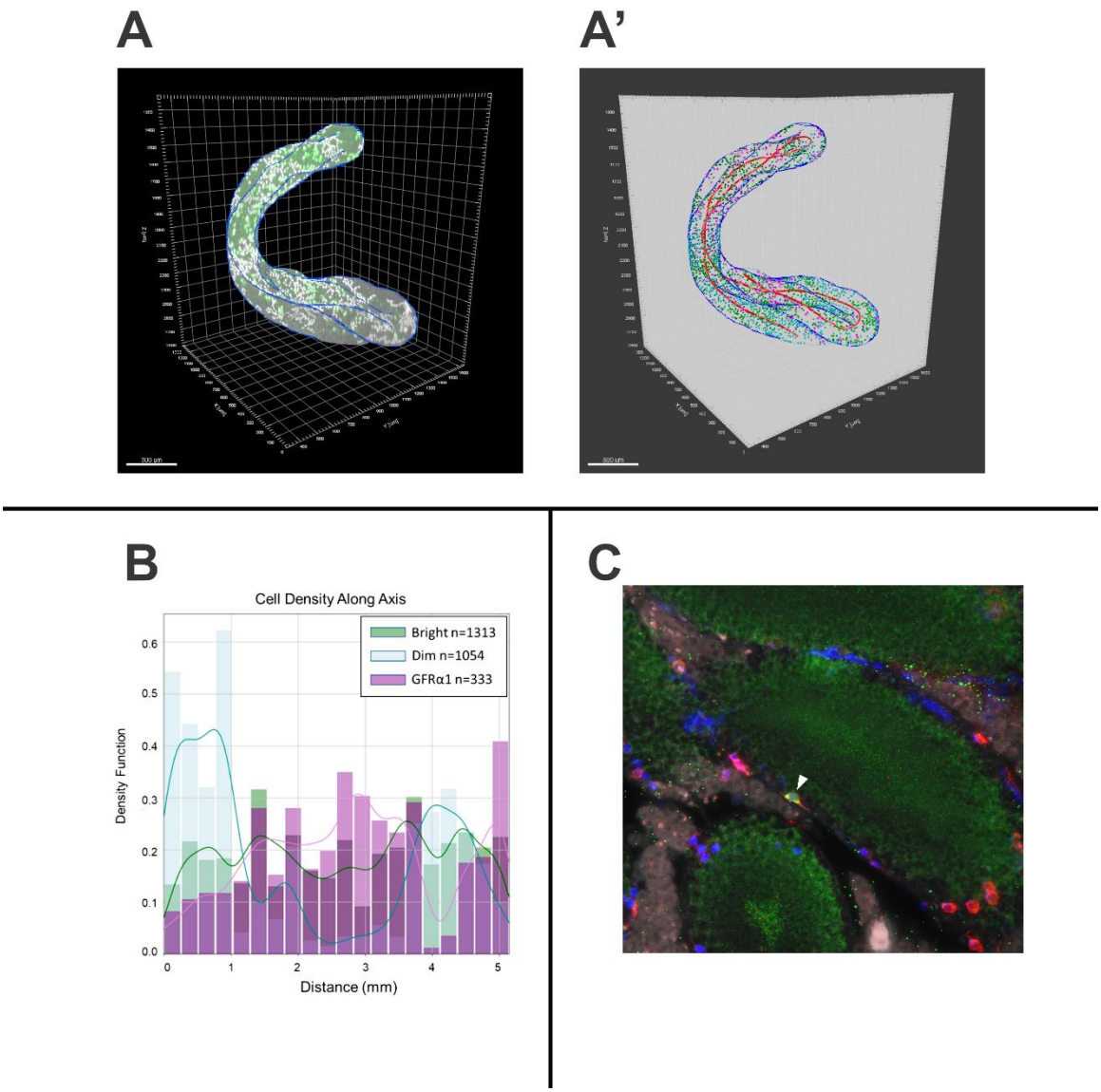

Figure 2.3. iDISCO/LSFM identifies SSC markers

A) 3D projection and (A') spot/surface identification (bright: green, dim: light blue, ZBTB16/GFRα1: purple) in a masked tubule (tubule: dark blue, axis: red).

B) Histogram and kernel density estimation of bright ZBTB16, dim ZBTB16, and ZBTB16/GFRα1 labeled cells in relation to the tubule axis.

C) 30um max intensity projection of optical sections (488nm background: white, GFP: green, GFRα1: red, ZBTB16: blue**,** arrowhead: ZBTB16^{+}/GFRα1^{+}/ID4^{+} cell

CHAPTER 3

G-Protein signaling accelerates stem cell divisions in *Drosophila* males

Manashree Malpe[*] Leon F. McSwain[*], Karl Kudyba[*], Chun L. Ng, Jennie Nicholson, Maximilian Brady, Yue Qian, Vinay Choksi, Alicia G. Hudson, Benjamin B. Parrott, and Cordula Schulz. 2019. *Submitted to: Scientific Reports*

ABSTRACT

Adult stem cells divide to renew the stem cell pool and replenish specialized cells that are lost due to death or usage. However, little is known about the mechanisms regulating how stem cells adjust to a demand for specialized cells. A failure of the stem cells to respond to this demand can have serious consequences, such as tissue loss, or prolonged recovery post injury.

Here, we challenge the male germline stem cells (GSCs) of *Drosophila melanogaster* for the production of specialized cells using mating experiments. We show that repeated mating reduced the sperm pool and accelerated germline stem cell (GSC) divisions. The increase in GSC divisions depended on the activity of the highly conserved G-proteins. Germline expression of RNA-Interference (RNA-*i*) constructs against G-proteins or a dominant negative G-protein eliminated the increase in GSC divisions in mated males. Consistent with a role for the G-proteins in the regulation of GSC divisions, RNA-*i* against seven out of 35 G-protein coupled receptors (GPCRs) within the germline cells also eliminated the capability of males to accelerate their GSC divisions in response to mating. Our data show that GSCs are receptive to GPCR stimulus, potentially through a network of interactions among multiple signaling pathways.

INTRODUCTION

Metazoan tissues undergo homeostasis wherein stem cells divide and their daughter cells proliferate and differentiate to replace lost cells. The human hematopoietic stem cells, for example, renew a remarkable number of about one trillion blood cells per day [1, 2]. Stem cells have to maintain a baseline mitotic

activity for the production of daughter cells that account for the daily turnover of differentiated cells. However, whether stem cells can modulate their mitotic activity in response to demands that challenge the system is not fully explored. In some instances, stem cells respond to physiological cues; for example, murine hematopoietic stem cells divide more frequently during pregnancy due to increased oestrogen levels [3]. In *Drosophila melanogaster*, intestinal stem cells initiate extra cell divisions upon ablation of differentiated gut cells. *Drosophila* GSCs modulate their mitotic activity in response to environmental conditions, such as nutrient availability and temperature [4-7].

Drosophila is an excellent model for identifying the molecules and mechanisms that regulate and fine-tune tissue homeostasis. A plethora of genetic tools are available for manipulating and monitoring dividing adult stem cells in *Drosophila*. The small size of the fly, the short generation cycle, and the fairly low costs covering their maintenance allow for high throughput screens. Here, we subjected several thousand male and several million virgin female flies to mating experiments, a task challenging to perform with vertebrate model organisms. We discovered that repeated mating caused a reproducible and significant increase in GSC division frequency in *Drosophila wild-type* (*wt*) males. Our analysis revealed that this response to mating was dependent on the activity G-proteins. Impairing G-protein activity from the germline cells eliminated the ability of the GSCs to increase their division frequency in response to mating.

G-proteins are highly conserved molecules that associate with GPCRs. GPCRs constitute a large family of cell surface receptors that mediate the cell's

response to a wide range of external stimuli, including odors, pheromones, hormones, and neurotransmitters. Loss of GPCR signaling affects countless developmental and neural processes in humans, as well as vertebrate and invertebrate model organisms [8-10]. Here we show that reducing the expression of seven out of 35 GPCRs via RNA-*i* from the germline cells eliminated the capability of males to accelerate their GSC divisions when mated. These were the Serotonin (5-HT) Receptors 1A, 1B and 7, Metuselah (Mth), Metuselah-like5 (Mth-l5), Octopamineβ2-Receptor (Octβ2R), and a predicted GPCR encoded by *CG12290*.

A role for any of these GPCRs in regulating GSC division frequency is novel. No previous study has identified any functional role for Mth-l5 or CG12290. Serotonin, Octopamine, and Mth signaling play opposing roles in life-span, locomotion, and sleep [11-16]. Mth signaling also regulates vesicle trafficking at the synapse, Octopamine signaling regulates ovulation, and Serotonin signaling plays essential roles in memory formation and learning [17-19].

RESULTS

Mating increased the percentage of GSCs in mitosis

As is typical for many stem cells, the *Drosophila* GSCs are found in a specific cellular microenvironment. They are located at the tip of the gonad, where they are attached to somatic hub cells (Figure 3.1A, A'). Upon GSC division, one of the daughter cells, called gonialblast, undergoes four rounds of stem cell daughter characteristic transit amplifying divisions, resulting in 16 spermatogonia. Subsequently, spermatogonia enter a tissue-specific

differentiation process. They grow in size, undergo the two rounds of meiosis, and develop through extensive morphological changes into elongated spermatids [20]. According to this tightly controlled homeostasis program, each GSC division can only produce 64 spermatids (Figure 3.1A). Thus, an increase in sperm production is reliant on the GSCs.

We investigate division frequency using an established immuno-fluorescence protocol [7]. In this approach, Vasa-positive GSCs are identified based on their position adjacent to FasciclinIII (FasIII)-positive hub cells (Figure 3.1A'). The percentage of GSCs in mitosis, the M-phase index (MI), is investigated by staining against phosphorylated Histone-H3 (pHH3). The MI of the GSCs (MI^{GSC}) is calculated by dividing the number of pHH3-positive GSCs by the total number of GSCs.

To investigate if stem cells can modulate their division frequency in response to a demand for specialized cells, we challenged *Drosophila* males in mating experiments. For each experiment, 80-100 males were exposed individually to virgin females. An equal number of male siblings were each kept in solitude and served as the non-mated controls. To keep experimental variation to a minimum, we employed a three-day mating protocol for all experiments, kept the animals under the same conditions, dissected the testes at the same time of the same day, and dissected experimental groups in tandem. Using *wt* males, we obtained robust and reproducible increases in MI^{GSC} in response to mating. The box-plot in Figure 3.1B shows the observed difference in MI^{GSC} between mated and non-mated populations of isogenized *wt*, *Oregon R* (*OR*), males from 17

independent mating experiments. Interestingly, we observed variability in MI^{GSC} among males of each condition. The MI^{GSC} of non-mated males ranged from six to nine percent, with a median at seven percent. The MI^{GSC} of mated males ranged from 11 to 18 percent, with a median at 16.5 percent. We hypothesize that this variability in MI^{GSC} within each condition is due to naturally occurring physiological differences within the flies. Likewise, the increase in MI^{GSC} in response to mating varied among the different experiments, but, in each of the experiments, the increase was biologically and statistically significant.

We next investigated if only a few males within a population contributed to the increase in MI^{GSC} or whether the effect of mating is reflected by changes in the MI^{GSC} across a population. These data are displayed in frequency distribution graphs (FDGs). FDGs show how often a particular value is represented within a population. When the distribution of the MI^{GSC} for testes within one population of *OR* flies was plotted, the resulting FDG revealed that mated males had significantly fewer testes with an MI^{GSC} of zero and more testes with higher MI^{GSC} compared to non-mated siblings (Figure 3.1C). We observed the same result for another isogenized *wt* strain, *Canton S* (*CS*, Figure 3.1D). We conclude that mating affected the MI^{GSC} of many males within one mated population.

Finally, we asked how long or frequently we had to mate the males to see an increase in MI^{GSC}. For this, we mated *OR* males to varying numbers of virgin females and subsequently analyzed how many of their GSCs were in mitotic division. When we exposed *OR* males for 24 hours to one (1F, 24 hrs), two (2F, 24 hrs), or three (3F, 24hrs) female virgins, no significant difference in MI^{GSC}

between non-mated and mated males was apparent (Figure S3.1 A). Robust and reproducible increases were seen in *OR* males that were exposed to three virgin females on each of two (2x3F, 48 hrs) or three (3x3F, 72 hrs) days of mating (Figure S3.1 1A). We conclude that males have to mate repeatedly for an increase in MI^{GSC} to occur. The increase in MI^{GSC} in mated males was reversible, showing that the response to mating was dynamic. Moving males back into solitude after the three-day mating experiment for 48 hours (3x3F, 120 hrs) eliminated the increase in MI^{GSC} (Figure S3.1 A). Control males mated for 120 hours (5x3F, 120 hrs), in contrast, still had a significant increase in MI^{GSC} (Figure S3.1 A).

Mating increased GSC division frequency

As another measure of cell divisions, we investigated the percentage of GSCs in synthesis phase (S-phase) of the cell cycle. Testes were labeled with 5-ethynyl-2'-deoxyuridine (EdU) and the S-phase index of the GSCs (SI^{GSC}) was calculated by dividing the number of EdU-positive GSCs by the total number of GSCs. Using pulse-labeling experiments, we observed that mated *OR* males displayed significant higher SI^{GSC} compared to their non-mated siblings (Figure 3.1E). Together with the increase in the MI^{GSC} this suggests that mating accelerates stem cell divisions.

To test this hypothesis, the lengths of the cell cycle were measured using EdU feeding experiments. In this approach, *OR* animals were fed EdU during the mating experiment. We then calculated how many GSCs had been in S-phase at different time points. Our EdU-incorporation experiment revealed that the number

of EdU-positive GSCs increased rapidly after 24 hours of feeding and reached 80% at 60 hours of feeding (Figure 3.1F). Prolonged feeding further increased the numbers of EdU-positive GSCs but this data was excluded from the study as the majority of males that were fed EdU while mating had died by 72 hours of the experiment. The response curve we obtained in this time-course experiment is different from the response curves reported by other groups that used bromo-deoxy-uridine (BrDU) as the thymidine analog instead of EdU. For example, the non-mated males in our experiment had about 70% of EdU-positive GSCs after 48 hours of feeding. A study using *white* (*w*) mutant animals fed the same concentration of the thymidine homologue had a steeper response curve, in which 85% of the GSCs were BrDU-marked after 48 hours of feeding [21]. Another study using *yellow, vermillion (y, v)* flies showed even steeper response curves where 100% of the GSCs were BrDU-labeled after 24 hours. However, in this study, animals were fed a 30 times higher concentration of the thymidine homologue than used in our study [22]. We propose that the different response curves are due to the different genetic backgrounds, chemicals and doses.

Most importantly, mated males had significantly more EdU-positive GSCs at 36 and 48 hours of mating compared to their non-mated siblings (Figure 3.1F). This experiment shows that, in mated males, more GSCs had entered S-phase of the cell cycle. We conclude that mated males had accelerated GSC divisions.

To further investigate how mating affects the cell cycle, we employed the Fly-Fucci technology in combination with the UAS-Ga4 expression system (Duffy, 2002 #321)(Phelps, 1998 #34)(Zielke, 2014 #1122). With Fly-Fucci, the coding

regions of fluorescent proteins are fused to the destruction boxes of cell cycle regulators, allowing the marking of different cell cycle stages. These artificial proteins are expressed under control of the Yeast Upstream Activating Sequences [23] (Zielke, 2014 #1122). UAS-controlled target genes can be expressed under spatial control using tissue-specific Gal4-transactivators. In addition, temporal control can be applied to their expression by exposing the flies to different temperatures (Phelps, 1998 #34)(Duffy, 2002 #321). For our experiments, we used a *nanos-Gal4*-transactivator (NG4) with a reported expression in GSCs, gonialblasts, and spermatogonia (Van Doren, 1998 #55). Using two independent Fucci-lines, we observed that MI^{GSC} did not significantly increase in mated *Fucci/NG4* males while mated controls animals (*Fucci/wt*) increased their MI^{GSC} compared to non-mated siblings (Figure S3.1 B). We conclude that expressing FUCCI-constructs from these fly lines within the GSCs interfered with their ability to significantly increase MI^{GSC} in response to mating. One possible explanation for this could be that the expression of proteins with destruction boxes could overload the cell cycle machinery of male GSCs.

Mating reduced the sperm pool

To confirm that our mating experiments created a demand for sperm, we explored differences in the sperm pool of the seminal vesicles between non-mated and mated males. For this, we used two different transgenic constructs that label the sperm. A Don Juan-Green Fluorescent Protein (DJ-GFP) reporter labels the sperm bodies and allows to assess the overall amount of sperm within the seminal vesicles [24]. A ProtamineB-GFP (Mst35B-GFP) line, on the other

hand, only labels the sperm heads and can be used to count the sperm within the seminal vesicles [25]. With each of these reporters, individualized mature sperm was normally seen within the seminal vesicle of the male reproductive tract.

According to the literature, the total number of sperm within one seminal vesicle varies among different *Drosophila* species and among genetic backgrounds [25-27]. To keep the genetic background consistent among our experiments, we crossed each of the reporter lines to *OR* females and used their male progeny for our mating experiments. The seminal vesicles were then analyzed at days one to three of the experiment. Based on the size and the fluorescence of the seminal vesicles, we first sorted them into three classes. Class 1 and class 2 seminal vesicles were completely filled with GFP-positive sperm heads. However, class 1 seminal vesicles were very wide (Figure 3.2A), while class 2 seminal vesicles were thinner (Figure 2B). Class 3 seminal vesicles contained only few GFP-positive sperm heads and had areas that were not filled with GFP (Figure 3.2C, arrows). A quantification revealed that non-mated males had mostly class 1 and 2 seminal vesicles, while mated males had mostly class 3 seminal vesicles. While we still detected class 1 and 2 seminal vesicles in males that had mated for only one day, their numbers were severely reduced in males after two and three days of mating (Figure 3.2D-F).

To further validate our observation that mating reduces the amount of sperm, we developed an automated procedure that calculates the volume occupied by Mst35B-GFP-positive sperm heads per seminal vesicle in all focal planes (voxels in Figure 3.2G). This allowed us to investigate larger numbers of

seminal vesicles compared to a previously reported method, in which images through the seminal vesicles were flattened and sperm heads counted by eye [25]. Furthermore, a computer-based calculation eliminates subjective bias introduced by the investigator. Based on our computer calculation, the sperm heads of mated males occupied significantly less volume within the seminal vesicles than the sperm in non-mated males (Figure 3.2G). Notably, the total volume occupied by sperm became more reduced with every day of mating. By days two and three of mating it ranged from 0.1 to 0.4 x 10^6 voxels per seminal vesicle. The non-mated sibling controls, in contrast, maintained a large GFP-occupied volume in their seminal vesicles, with an average of 1.2 x 10^6 voxels per seminal vesicle. The computer program estimated the numbers of sperm per seminal vesicle of non-mated males around 2000, while males that were mated for two or three days had less than 500 sperm in their seminal vesicles. As our mated males showed a drastic reduction in sperm, we argue that we have created a demand for sperm.

Mating had no effect on GSC numbers

It was previously reported that females significantly increased the numbers of their GSCs upon mating [28]. According to the literature, an adult male gonad contains up to twelve GSCs per testis, but the exact number of GSCs per testes appears to vary among different strains and laboratories. One study using a *wt* strain of males reported six to ten GSCs per testis, while other studies using transgenic males in a *w* mutant genetic background reported 8.94 and 12.3 GSCs per testis, respectively [29-31]. Among our fly lines, we found variation in

GSC numbers as well. The distribution of GSCs ranged from one to 14 per testis, with an average of seven GSCs per testis. Males from an isogenized *OR* stock had the lowest average number of GSCs, having only four to five GSCs per testis (Figure 3.3A). Males from an isogenized *CS* stock had an average of six GSCs per testis (Figure 3.3B). Animals mutant for *w* alleles, w^{1118} and w^{1}, had on average eight and seven GSCs per testis, respectively (Figures 3.3 C, D). Males from a v^{1}, y^{1} stock, which serves as the genetic background for many RNA-*i* lines, had the highest average number of GSCs, at 11 GSCs per testis (Figure 3.3E). We believe that the obtained GSC numbers are specific to the fly lines in our laboratory and do not necessarily reflect the numbers of GSCs in fly stocks of other laboratories.

Importantly, we did not observe a significant difference in the numbers of GSCs between non-mated and mated siblings in any of these fly lines (Figure 3.3A-E). We concluded that mating did not affect the numbers of GSCs in our fly stocks. However, the observed variation in GSC numbers prompted us to perform our experiments in animals from as similar genetic backgrounds as possible. All males reported in the following of this manuscript carried the X-chromosome from our isogenized *OR* line.

The increase in MI^{GSC} upon mating required G-protein signaling

Drosophila mating is a complex and genetically controlled behavior that is dependent on neural circuits [32]. This implicates a possible neuronal control in regulating GSC divisions during mating. Therefore, we wanted to focus on the type of signaling pathway commonly stimulated during neural activity, G-protein

signaling [33, 34]. In a non-stimulated cell, a trimeric complex of G-proteins, G_α, G_β, and G_γ is associated with classical GPCRs (Figure 3.4A, step 1). When ligand binds to the GPCR, a guanidyl exchange factor within the GPCR becomes activated that exchanges GDP for GTP in the G_α subunit. The exchange leads to the dissociation of G_α and the $G_{\beta/\gamma}$ complex from each other and from the GPCR. Remaining attached to the membrane, G_α and $G_{\beta/\gamma}$ diffuse along it and activate downstream signal transducers (Figure 3.4A, step 2) [35, 36]. Most organisms have multiple genes that encode for each of the G-protein subunits. *Drosophila* has six G_α, three G_β, and two G_γ proteins, yet only a few examples are available in the literature associating a specific *Drosophila* G-protein with an upstream GPCR [35, 37].

Animals mutant for G-protein subunits are often lethal, making it problematic to investigate their roles in the adult. Furthermore, studying G-protein signaling in animals lacking their function throughout the whole body may could affect behavior and physiology of the fly, leading to confounding effects on mating and GSC divisions. Fortunately, large collections of RNA-*i*-lines are available that are expressed under control of UAS. To reduce G-protein signaling we employed two separate *nanos*-Gal4-transactivators (*NG4*), *NG4-1* and *NG4-2.* When RNA-*i* against the different G-protein subunit was expressed within the germline cells via *NG4-1*, several of the mated males displayed only a weak increase in MI^{GSC} compared to their non-mated siblings (Table 3.1). We focused on an RNA-*i*-line that is directed against the subunit $G_\alpha i$ as animals expressing this construct within the germline did not show any increase in MI^{GSC} in response

to mating (Table 3.1). For reproducibility, we conducted each of the following experiments in triplicates. We used progeny from transgenic Gal4 and UAS-flies that had been crossed to *wt* as positive controls. As expected, each population of positive control males displayed a significant increase in MI^{GSC} when mated (Figure 3.4B). Experimental flies expressing $G_{\alpha}i$-*i* via *NG4-1* or *NG4-2*, however, failed to increase MI^{GSC} (Figure 3.4C).

We next sought to validate the role for G-protein signaling in GSC division frequency by an alternative approach. A dominant negative version of *Drosophila* $G_{\gamma}1$ ($dnG_{\gamma}1$) is available that serves as a reliable tool to abolish G-protein signaling [38]. Males expressing $dnG_{\gamma}1$ via either *NG4-1* or *NG4-2* did not show an increase in MI^{GSC} in response to mating (Figure 3.3C). Control $dnG_{\gamma}1$/*wt* animals, on the other hand, had increased MI^{GSC} upon mating (Figure 3.3B). These data clearly show that signaling via G-proteins is required for the increase in MI^{GSC}. Plotting the results in FDGs confirmed that mated control animals had significantly fewer testes with an MI^{GSC} of zero and more testes with higher MI^{GSC} compared to non-mated males (Figures S3.3 A-D), and that this response to mating was eliminated in experimental males (Figures S3.3 E-H).

In mammalian cells, three major G-protein-dependent signaling cascades have been described (Figure 3.3A, steps 3a, b, c) [33, 39]. For *Drosophila*, the literature provides little information on the signaling cascades downstream of GPCRs but it is generally assumed that the mammalian signal transducers are conserved in flies. To further validate that an increase in MI^{GSC} upon mating is regulated by G-protein signaling we expressed RNA-*i* and mis-expression

constructs for conserved signal transducers via NG4 and found that males expressing RNA-*i*-lines for one of the *Drosophila Protein Kinase C* (*PKC*) proteins, *PKC98E*, for *Inositol-triphosphate 3-Kinase* (*IP3K),* and for *Ca2+/Calmodulin-dependent protein kinase II (CaMKII)* indeed failed to increase MI^{GSC} in response to mating (Table 3.1).

RNA-i against seven distinct GPCRs blocked the increase in MI^{GSC} upon mating

To further confirm that G-protein signaling regulates the increase in MI^{GSC} we aimed towards identifying the upstream GPCRs. Next Generation Sequencing (NGS) of RNA from *wt* testis tips revealed the expression of 140 receptors, including 35 classical GPCRs (Figure 3.5 and Table 3.2). The functions of many of these GPCRs have not been studied yet and mutant animals are only available in rare cases. Expressing RNA-*i*-constructs against most GPCRs in the germline had little to no effect on the ability of the GSCs to increase their MI^{GSC} in response to mating (Table 3.2). RNA-*i* against three Serotonin Receptors (5HT-1A, 5HT-1B and 5HT-7), Mth, Mth-l5, Octβ2R, and a predicted GPCR encoded by CG12290, clearly and reproducibly eliminated this ability. Animals carrying UAS-controlled RNA-*i*-constructs against these GPCRs (*GPCR-i*) were crossed to *wt*, *NG4-1* and *NG4-2*, and MI^{GSC} of their progeny was investigated. Each of the controls (*GPCR-i/wt*) increased their MI^{GSC} when repeatedly mated to females in each of the triplicate experiments (Figure 3.5A and Figures S3.3 A-G). However, when the *GPCR-i*-animals were crossed with either *NG4-1* (Figure 5B and Figures S3.3 H-N) or *NG4-2* (Figure 3.5C and

Figures S3.3 O-U) the MI^{GSC} of their non-mated and mated progeny did not significantly differ. Confirming the necessity of the GPCRs in increasing MI^{GSC}, we investigated alternative RNA-*i*-lines. A second RNA-*i*-line for Mth blocked the increase in MI^{GSC} in mated males and a second RNA-*i*-line for 5HT-1A displayed only a weak response to mating (Table 3.3).

Mating success was evaluated by two criteria: visual observation and the appearance of progeny. When flies were anesthetized to exchange the females for fresh virgins, several copulating pairs of males and females were always observed. Furthermore, 100 single females that had been exposed to males on day one of the experiment were placed into one food vial each and mating success evaluated a few days later by counting the percentage of vials with progeny. Most males in this study sired 60-90% of the females. Specifically, each of the *GPCR-i/NG4-1* males produced offspring (Table S3.1), showing that a block in the increase in MI^{GSC} is not caused by a failure to mate but by a lack of GPCR signaling. Viable alleles of 5HT-1A and 5HT-1B were not pursued as alternative strategies because they displayed only a weak mating success rate (Table S3.1).

Finally, we wanted to assure that male age had no effect on the increase in MI^{GSC}. We performed a time-course experiment of one, two, three, and four-week old *OR* males. We found that mated males of all ages showed robust increases in MI^{GSC} compared to their non-mated siblings (Figure S3.1 C). We conclude that aging animals for up to four weeks had little to no effect on the ability of *wt* GSCs to increase their MI^{GSC} in response to mating, and that the age

of the transgenic animals used in this study (three weeks of age at the time of testes dissection) had no impact on the obtained results.

DISCUSSION

Here, we show that repeated mating reduced the sperm pool and increased GSC division frequency. Using highly controlled experiments, we demonstrate that mated males had more GSCs in M-phase and S-phase of the cell cycle compared to non-mated males. Mated males also showed faster incorporation of EdU indicating that their GSCs progressed faster through the cell cycle. Our findings demonstrate that GSCs can respond to a demand for sperm by accelerating their mitotic activity. Based on RNA-*i* targeting G-proteins and a dominant negative construct against $G_{\gamma}1$, the increase in MI^{GSC} of mated males is dependent on G-protein signaling. Furthermore, signal transducers predicted to act downstream of G-proteins and GPCRs predicted to act upstream of G-proteins also appeared to be required for the response to mating.

Due to the lack of mutants and a potential interference of whole animal knock-down in the behavior of the flies, we used tissue-specific expression of RNA-*i*-constructs. It is surprising that our studies revealed potential roles for seven instead of a single GPCR in the increase of MI^{GSC} in response to mating. A possible explanation is that some of the RNA-*i*-lines have off-target effects. RNA-*i*-hairpins can cause the down-regulation of unintended targets due to stretches of sequence homologies, especially when long hairpins are used [40, 41]. However, with the exception of the RNA-*i*-line directed against 5HT-7, all lines that produced a phenotype contain second generation vectors with a short, 21

nucleotide hairpin predicted to have no off-target effects [42]. We hypothesize that multiple GPCRs regulate the increase in MI^{GSC} in response to mating. Consistent with this, expression of second RNA-*i*-line directed against Mth or 5HT-1A interfered with the increase in MI^{GSC} in mated males.

Our finding that RNA-*i* against several GPCRs blocked the increase in MI^{GSC} in mated males suggests a high level of complexity in the regulation of GSC divisions. In the literature, increasing evidence has emerged that GPCRs can form dimers and oligomers and that these physical associations have a variety of functional roles, ranging from GPCR trafficking to modification of G-protein mediated signaling [43-45]. In *C. elegans,* two Octopamine receptors, SER-3 and SER-6, additively regulate the same signal transducers for food-deprived-mediated signaling. One possible explanation for the non-redundant function of the two receptors was the idea that they form a functional dimer [46]. In mammalian cells, 5-HT receptors can form homo-dimers and hetero-dimers and, dependent on this, have different effects on G-protein signaling [47-49]. In cultured fibroblast cells, for example, G-protein coupling is more efficient when both receptors within a 5-HT4 homo-dimer bind to agonist instead of only one [50]. In cultured hippocampal neurons, hetero-dimerization of 5-HT1A with 5-HT7 reduces G-protein activation and decreases the opening of a potassium channel compared to 5-HT1A homo-dimers [51]. The formation of hetero-dimers of GPCRs with other types of receptors plays a role in depression and in the response to hallucinogens in rodents [52, 53].

Alternatively, or in addition to the possibility that some or all of the seven GPCRs form physical complexes, a role for several distinct GPCRs in regulating GSC division frequency could be explained by crosstalk among the downstream signaling cascades. One signaling cascade could, for example, lead to the expression of a kinase that is activated by another cascade. Similarly, one signaling cascade could open an ion channel necessary for the activity of a protein within another cascade. Unfortunately, the literature provides little information on *Drosophila* GPCR signal transduction cascades and only very few mutants have been identified that affect a process downstream of GPCR stimulation. Thus, it remains to be explored how stimulation of the GPCRs and G-proteins increase GSC divisions.

The role for G-protein signaling in regulating the frequency of stem cell divisions is novel. Our data suggest that the increase in MI^{GSC} in response to mating is regulated by external signals, potentially arising from the nervous system, that stimulate G-protein signaling within the GSCs. Based on the nature of the GPCRs, the activating signal could be Serotonin, the Mth ligand, Stunted, Octopamine, or two others, yet unknown, signals that activate Mth-l5, and CG12290 [54-56]. It will be interesting to address which of these ligands are sufficient to increase MI^{GSC}, in what concentrations they act, by which tissues they are released, and whether they also affect other stem cell populations.

Methods

Fly husbandry

Flies were raised on a standard cornmeal/agar diet and maintained in temperature-, light-, and humidity-controlled incubators. Unless otherwise noted, all mutations, markers, and transgenic lines are described in the *Drosophila* database and were obtained from the Bloomington stock center (Consortium, 2003 #132).

UAS/Gal4-expression studies

Two separate X; UAS-*dicer*; nanos-*Gal4* (NG4-1 and NG4-2) fly lines were used as transactivators. Females from the transactivator line or *wt* females were crossed with males carrying target genes under the control of UAS in egg lay containers with fresh apple juice-agar and yeast paste to generate either experimental or control flies. The progeny were transferred into food bottles, raised to adulthood at 18°C, males collected and then shifted to 29°C for seven days to induce high activity of Gal4 prior to the mating experiment. Note that the males were not collected as virgins as to avoid any potential developmental or learning effects on our experiments.

Mating experiments

Unless otherwise noted, mating experiments were performed at 29°C. Males and virgin females were placed on separate apple juice-agar plates with yeast paste overnight to assure they were well fed prior to their transfer into mating chambers. Single males were placed into each mating slot either by themselves (non-mated) or with three virgin females (mated) and the chambers

closed with apple juice-agar lids with yeast paste. Females were replaced by virgin females on each of the following two days and apple juice-agar lids with yeast paste were replaced on a daily basis for both non-mated and mated animals. In most instances, females from the stock *X^X*, *y, w, f* / Y / *shi ts* were used as virgins. When raised at 29°C, only females hatch from this stock. For fertility tests, *OR* virgins were used. Note that 10-20% of the mated males died during the experiment while only 5% of the non-mated siblings died.

Immuno-fluorescence and microscopy

Animals were placed on ice to immobilize them. Gonads were dissected in Tissue Isolation Buffer (TIB) and collected in a 1.5 ml tube with TIB buffer on ice for no more than 30 minutes. Gonads were then fixed, followed by immuno-fluorescence staining and imaging as previously described [7]. The mouse anti-FasciclinIII (FasIII) antibody (1:10) developed by C. Goodman was obtained from the Developmental Studies Hybridoma Bank, created by the NICHD of the NIH and maintained at The University of Iowa, Department of Biology, Iowa City, IA 52242. Goat anti-Vasa antibody (1:50 to 1:300) was obtained from Santa Cruz Biotechnology Inc. (sc26877), anti-phosphorylated Histone H3 (pHH3) antibodies (1:100 to 1:1000) were obtained from Fisher (PA5-17869), Milllipore (06-570), and Santa Cruz Biotechnology Inc. (sc8656-R). Secondary Alexa 488, 568, and 647-coupled antibodies (1:1000) and Slow Fade Gold embedding medium with DAPI were obtained from Life Technologies. Images were taken with a Zeiss Axiophot, equipped with a digital camera, an apotome, and Axiovision Rel.

software. Statistical relevance was determined using the two-tailed Graphpad student's t-test.

EdU-labeling experiments

The EdU-labeling kit was obtained from Invitrogen and the procedure performed following manufacturer's instructions. For EdU-pulse labeling experiments, animals were mated as described above, and the dissected testes incubated with 10mM EdU in PBS for 30 minutes at room temperature prior to fixation. For EdU-feeding experiments, *OR* males were fed 10 mM EdU in liquid yeast provided on paper towels. These animals were mated at room temperature (21°C) because the paper towels easily dried out at higher temperatures, causing the flies to dehydrate and die.

Sperm head volumetric calculations

In order to easily evaluate sperm numbers, we turned to computer analysis in Python. By quantifying the volume of GFP signal we generated estimates to the amount of sperm in each seminal vesicle. Image stacks were taken of individual seminal vesicles. After masking relevant regions, each image set was normalized by mean subtraction and division by the standard deviation, followed by rescaling image intensity to encompass the range of the image. To remove signal noise, a median filter was applied and the mask refined by Otso thresholding. We determined signal volume by hysteresis thresholding. This approach initially thresholds an image at an upper limit, and then expands the region by adjacent pixels satisfying the lower threshold. We set the lower bound at the value generated from a triangle threshold and the upper threshold as the

median value above the lower limit. The number of signal voxels was calculated and normalized to an expected size of a single sperm head. Our analysis utilized OpenCV 3.4.2, Scipy1.2.1, Scikit-image 0.14.2, Numpy 1.16.2, Matplotlib 3.0.3, Seaborn 0.9.0, as well as built in Python 3.7.3 modules [57-61].

Acknowledgements

The authors dedicate this manuscript to Bruce Baker, who was one of the foremost scientists in the field, and a great colleague and friend. The authors are grateful to Richard Zoller, Yue Qian, Megan Aarnio, Heather Kudyba, Jacqueline Uribe, Chidemman Ihenacho, Stefani Moore, Sampreet Reddy, Amanda Cameron, Chederli Belongilot, Dylan Ricke, Kenneth Burgess, Amanda Redding, Erin Guillebeau, Jennifer Murphy, Chantel McCarty, Sarah Murphy, Haley Grable, Mitch Hanson, Haein Kim, and Sarah Rupert for technical assistance. We thank Bruce Baker, Carmen Robinett, Edward Kravitz, Matthew Freeman, Mark Brown, Erika Matunis, Steve DiNardo, Margaret Fuller, Alan Spradling, Hannele Rahuola-Baker, Eric Bohman, Celeste Berg, Wolfgang Lukowitz, Patricia Moore, Jim Lauderdale, Michael Tiemeyr, Scott Dougan, Rachel Roberts-Galbraith, and Rhonda Snook for helpful discussions, and Heath Aston Zachary Letts for comments on the manuscript. We are especially grateful to Barry Ganetzky for the *X^X, shi^{ts}* fly stock and to Wolfgang Lukowitz for the use of his microscope. This work was supported by NSF grants #0841419 and #1355009, and UGA bridge funds given to CS.

Author contributions

M.M, B.B.P, and C.S developed and supervised the project, L.F.M coordinated the mating experiments, K.K. identified the GPCRs expressed in testes tips and developed the computer analysis for the sperm counts, all authors performed the experiments, M.M, K.K., and CS wrote the manuscript.

Competing interests

The authors declare no competing interests.

References

1. Dancey, J.T., Deubelbeiss, K.A., Harker, L.A. & Finch, C.A. Neutrophil kinetics in man. *J Clin Invest* **58**, 705-715 (1976).
2. Erslev, A. Production of erythrocytes, in *Hematology*. (ed. B.E. William WJ, Erslev AJ, Lichtman MA) 365-376 (

Mc-Graw-Hill, New York, NY; 1983).

3. Nakada, D. *et al.* Oestrogen increases haematopoietic stem-cell self-renewal in females and during pregnancy. *Nature* **505**, 555-558 (2014).
4. Hsu, H.J., LaFever, L. & Drummond-Barbosa, D. Diet controls normal and tumorous germline stem cells via insulin-dependent and -independent mechanisms in Drosophila. *Dev Biol* **313**, 700-712 (2008).
5. Amcheslavsky, A., Jiang, J. & Ip, Y.T. Tissue damage-induced intestinal stem cell division in Drosophila. *Cell Stem Cell* **4**, 49-61 (2009).
6. McLeod, C.J., Wang, L., Wong, C. & Jones, D.L. Stem cell dynamics in response to nutrient availability. *Curr Biol* **20**, 2100-2105 (2010).
7. Parrott, B.B., Hudson, A., Brady, R. & Schulz, C. Control of germline stem cell division frequency--a novel, developmentally regulated role for epidermal growth factor signaling. *PLoS One* **7**, e36460 (2012).
8. Schoneberg, T. *et al.* Mutant G-protein-coupled receptors as a cause of human diseases. *Pharmacol Ther* **104**, 173-206 (2004).
9. Wettschureck, N. & Offermanns, S. Mammalian G proteins and their cell type specific functions. *Physiol Rev* **85**, 1159-1204 (2005).

10. Langenhan, T. *et al.* Model Organisms in G Protein-Coupled Receptor Research. *Mol Pharmacol* **88**, 596-603 (2015).
11. Lin, Y.J., Seroude, L. & Benzer, S. Extended life-span and stress resistance in the Drosophila mutant methuselah. *Science* **282**, 943-946 (1998).
12. Selcho, M., Pauls, D., El Jundi, B., Stocker, R.F. & Thum, A.S. The role of octopamine and tyramine in Drosophila larval locomotion. *J Comp Neurol* **520**, 3764-3785 (2012).
13. Silva, B., Goles, N.I., Varas, R. & Campusano, J.M. Serotonin receptors expressed in Drosophila mushroom bodies differentially modulate larval locomotion. *PLoS One* **9**, e89641 (2014).
14. Crocker, A. & Sehgal, A. Octopamine regulates sleep in drosophila through protein kinase A-dependent mechanisms. *J Neurosci* **28**, 9377-9385 (2008).
15. Yuan, Q., Joiner, W.J. & Sehgal, A. A sleep-promoting role for the Drosophila serotonin receptor 1A. *Curr Biol* **16**, 1051-1062 (2006).
16. Li, Y. *et al.* Octopamine controls starvation resistance, life span and metabolic traits in Drosophila. *Sci Rep* **6**, 35359 (2016).
17. Song, W. *et al.* Presynaptic regulation of neurotransmission in Drosophila by the g protein-coupled receptor methuselah. *Neuron* **36**, 105-119 (2002).

18. Lee, H.G., Seong, C.S., Kim, Y.C., Davis, R.L. & Han, K.A. Octopamine receptor OAMB is required for ovulation in Drosophila melanogaster. *Dev Biol* **264**, 179-190 (2003).

19. Sitaraman, D. *et al.* Serotonin is necessary for place memory in Drosophila. *Proc Natl Acad Sci U S A* **105**, 5579-5584 (2008).

20. Fuller, M.T. Spermatogenesis, in *The development of Drosophila melanogaster*, Vol. 1. (ed. M. Bate, Martinez-Arias, A) 71-147 (Cold Spring Harbor Press, Cold Spring Harbor; 1993).

21. Wallenfang, M.R., Nayak, R. & DiNardo, S. Dynamics of the male germline stem cell population during aging of Drosophila melanogaster. *Aging Cell* **5**, 297-304 (2006).

22. Yang, H. & Yamashita, Y.M. The regulated elimination of transit-amplifying cells preserves tissue homeostasis during protein starvation in Drosophila testis. *Development* **142**, 1756-1766 (2015).

23. Abdouh, M., Albert, P.R., Drobetsky, E., Filep, J.G. & Kouassi, E. 5-HT1A-mediated promotion of mitogen-activated T and B cell survival and proliferation is associated with increased translocation of NF-kappaB to the nucleus. *Brain Behav Immun* **18**, 24-34 (2004).

24. Santel, A., Blumer, N., Kampfer, M. & Renkawitz-Pohl, R. Flagellar mitochondrial association of the male-specific Don Juan protein in Drosophila spermatozoa. *J Cell Sci* **111 (Pt 22)**, 3299-3309 (1998).

25. Tirmarche, S. *et al.* Drosophila protamine-like Mst35Ba and Mst35Bb are required for proper sperm nuclear morphology but are dispensable for male fertility. *G3 (Bethesda)* **4**, 2241-2245 (2014).

26. Pitnick, S., Markow, T.A. Male gametic Strategies: Sperm Size, Testes Size, and the Allocation of Ejaculate among Successive Mates by the Sperm-Limited Fly Drosophila Pachea and its Relatives. *The American Naturalist* **143**, 785-819 (1994).

27. Kubrak, O.I., Kucerova, L., Theopold, U., Nylin, S. & Nassel, D.R. Characterization of Reproductive Dormancy in Male Drosophila melanogaster. *Front Physiol* **7**, 572 (2016).

28. Ameku, T. & Niwa, R. Mating-Induced Increase in Germline Stem Cells via the Neuroendocrine System in Female Drosophila. *PLoS Genet* **12**, e1006123 (2016).

29. Chen, D. *et al.* Gilgamesh is required for the maintenance of germline stem cells in Drosophila testis. *Sci Rep* **7**, 5737 (2017).

30. Yamashita, Y.M., Jones, D.L. & Fuller, M.T. Orientation of asymmetric stem cell division by the APC tumor suppressor and centrosome. *Science* **301**, 1547-1550 (2003).

31. Sheng, X.R. & Matunis, E. Live imaging of the Drosophila spermatogonial stem cell niche reveals novel mechanisms regulating germline stem cell output. *Development* **138**, 3367-3376 (2011).

32. Manoli, D.S., Fan, P., Fraser, E.J. & Shah, N.M. Neural control of sexually dimorphic behaviors. *Curr Opin Neurobiol* **23**, 330-338 (2013).

33. Geppetti, P., Veldhuis, N.A., Lieu, T. & Bunnett, N.W. G Protein-Coupled Receptors: Dynamic Machines for Signaling Pain and Itch. *Neuron* **88**, 635-649 (2015).

34. Lee, D. Global and local missions of cAMP signaling in neural plasticity, learning, and memory. *Front Pharmacol* **6**, 161 (2015).

35. McCudden, C.R., Hains, M.D., Kimple, R.J., Siderovski, D.P. & Willard, F.S. G-protein signaling: back to the future. *Cell Mol Life Sci* **62**, 551-577 (2005).

36. Oldham, W.M. & Hamm, H.E. Heterotrimeric G protein activation by G-protein-coupled receptors. *Nat Rev Mol Cell Biol* **9**, 60-71 (2008).

37. Boto, T., Gomez-Diaz, C. & Alcorta, E. Expression analysis of the 3 G-protein subunits, Galpha, Gbeta, and Ggamma, in the olfactory receptor organs of adult Drosophila melanogaster. *Chem Senses* **35**, 183-193 (2010).

38. Deshpande, G., Godishala, A. & Schedl, P. Ggamma1, a downstream target for the hmgcr-isoprenoid biosynthetic pathway, is required for releasing the Hedgehog ligand and directing germ cell migration. *PLoS Genet* **5**, e1000333 (2009).

39. Moolenaar, W.H. G-protein-coupled receptors, phosphoinositide hydrolysis, and cell proliferation. *Cell Growth Differ* **2**, 359-364 (1991).

40. Kulkarni, M.M. *et al.* Evidence of off-target effects associated with long dsRNAs in Drosophila melanogaster cell-based assays. *Nat Methods* **3**, 833-838 (2006).

41. Moffat, J., Reiling, J.H. & Sabatini, D.M. Off-target effects associated with long dsRNAs in Drosophila RNAi screens. *Trends Pharmacol Sci* **28**, 149-151 (2007).

42. Perkins, L.A. *et al.* The Transgenic RNAi Project at Harvard Medical School: Resources and Validation. *Genetics* **201**, 843-852 (2015).

43. Filizola, M. & Weinstein, H. The study of G-protein coupled receptor oligomerization with computational modeling and bioinformatics. *FEBS J* **272**, 2926-2938 (2005).

44. Milligan, G. G protein-coupled receptor dimerisation: molecular basis and relevance to function. *Biochim Biophys Acta* **1768**, 825-835 (2007).

45. Terrillon, S. & Bouvier, M. Roles of G-protein-coupled receptor dimerization. *EMBO Rep* **5**, 30-34 (2004).

46. Yoshida, M., Oami, E., Wang, M., Ishiura, S. & Suo, S. Nonredundant function of two highly homologous octopamine receptors in food-deprivation-mediated signaling in Caenorhabditis elegans. *J Neurosci Res* **92**, 671-678 (2014).

47. Lukasiewicz, S. *et al.* Hetero-dimerization of serotonin 5-HT(2A) and dopamine D(2) receptors. *Biochim Biophys Acta* **1803**, 1347-1358 (2010).

48. Herrick-Davis, K. Functional significance of serotonin receptor dimerization. *Exp Brain Res* **230**, 375-386 (2013).

49. Xie, Z., Lee, S.P., O'Dowd, B.F. & George, S.R. Serotonin 5-HT1B and 5-HT1D receptors form homodimers when expressed alone and heterodimers when co-expressed. *FEBS Lett* **456**, 63-67 (1999).

50. Pellissier, L.P. *et al.* G protein activation by serotonin type 4 receptor dimers: evidence that turning on two protomers is more efficient. *J Biol Chem* **286**, 9985-9997 (2011).

51. Renner, U. *et al.* Heterodimerization of serotonin receptors 5-HT1A and 5-HT7 differentially regulates receptor signalling and trafficking. *J Cell Sci* **125**, 2486-2499 (2012).

52. Borroto-Escuela, D.O., Tarakanov, A.O. & Fuxe, K. FGFR1-5-HT1A Heteroreceptor Complexes: Implications for Understanding and Treating Major Depression. *Trends Neurosci* **39**, 5-15 (2016).

53. Moreno, J.L., Holloway, T., Albizu, L., Sealfon, S.C. & Gonzalez-Maeso, J. Metabotropic glutamate mGlu2 receptor is necessary for the pharmacological and behavioral effects induced by hallucinogenic 5-HT2A receptor agonists. *Neurosci Lett* **493**, 76-79 (2011).

54. Saudou, F., Boschert, U., Amlaiky, N., Plassat, J.L. & Hen, R. A family of Drosophila serotonin receptors with distinct intracellular signalling properties and expression patterns. *EMBO J* **11**, 7-17 (1992).

55. Cvejic, S., Zhu, Z., Felice, S.J., Berman, Y. & Huang, X.Y. The endogenous ligand Stunted of the GPCR Methuselah extends lifespan in Drosophila. *Nat Cell Biol* **6**, 540-546 (2004).

56. Maqueira, B., Chatwin, H. & Evans, P.D. Identification and characterization of a novel family of Drosophila beta-adrenergic-like octopamine G-protein coupled receptors. *J Neurochem* **94**, 547-560 (2005).

57. van der Walt, S., Colbert, C., Varoquaux, G. The NumPy Array: A Structure for Efficient Numerical Vomputation. *Computing in Science and Engineering*, 22-30 (2011).

58. van der Walt, S., Schoenberger, J.L., Nunez-Iglesias, J., Boulogne, F., Warner, J.D., Yager, N., Gouillart, E., Yu, T., and the scikit-image contributors scikit-image: Image processing in Python. *PerJ:e453* (2014).

59. Travis, E., Oliphant, E. A guide to NumPy. (2006).

60. Hunter, J.D. Matplotib: A 2D Graphics Environment. *Computing in Science and Engineering*, 90-95 (2007).

61. Jones, E., Oliphant, E., Peterson, P., *et al* SciPy: Open Source Scientific Tools for Python. (2001-).

Table 3.1. MI^{GSC} from control, RNA-*i* and overexpression lines directed against G-protein subunits and other signal transducers

UAS-driven expression for the listed genes in the germline via *NG4-1*. BL #: Bloomington stock number, Single and Mated: number of pHH3-positive GSCs/total number of GSCs = MI^{GSC}, Diff: MI^{GSC} of mated males minus MI^{GSC} of non-mated males. For RNA-*i*-lines marked by asterisks siblings outcrossed to *wt* did not show a strong response to mating either, suggesting leakiness of the lines.

Genotype	**BL#**	**Crossed to:**	**MI^{GSC} Single**	**MI^{GSC} Mated**	**Diff.**
UAS-G_{α}f-i	43201	NG4-1	19/448=4.2%	52/452=11.5%	7.3
	25930*	NG4-1	54/1031=5.2%	76/1183=6.1%	0.9
UAS-G_{α}i-i	34924	NG4-1	22/335=6.6%	49/322=15.2%	8.6
	40890	NG4-1	33/597=5.5%	59/536=11%	5.5
	31133	NG4-1	5/269=1.9%	19/285=6.7%	4.8
UAS-G_{α}o-i	34653*	NG4-1	23/313=7.3%	26/295=8.8%	1.5
	28010	NG4-1	18/240=7.5%	27/231=11.7%	4.2
UAS-G_{α}q-i	36820	NG4-1	24/403=6.0%	32/268=11.9%	5.9
	33765	NG4-1	33/320=10%	50/298=16.8%	6.8
	36775	NG4-1	9/153=5.9%	21/255=8.6%	2.7
	31268	OR	17/233=7.3	15/169=8.9	1.6
		OR	14/335=4.2	12/164=7.3	3.1
		OR	31/568=5.5	27/333=8.1	2.6

		NG4-1	25/556=4.5	8/296=2.7	-2.8
		NG4-1	23/332=6.9	23/291=7.9	1
		NG4-1	23/542=4.2	19/577=3.3	-0.9
		NG4-1	71/1430=5.0	50/1164=4.3	-0.7
	30735	NG4-1	14/318=4.4%	23/293=7.8%	3.4
UAS-G$_{\alpha}$s-i	29576	NG4-1	49/605=8.1%	60/615=9.7%	1.6
	50704	NG4-1	82/1137=7.3%	121/1527=7.9 %	0.6
UAS-G$_{\beta}$5-i	28310	NG4-1	10/306=3.3%	20/292=6.9%	3.6
UAS-G$_{\beta}$13F-i	35041	NG4-1	38/752=4.8%	46/785=5.7%	0.9
	31134	NG4-1	12/198=6%	31/221=14%	8.0
UAS-G$_{\beta}$76C-i	28507	NG4-1	14/219=6.4%	26/226=11.5%	5.1
UAS-G$_{\gamma}$1-i	25934	NG4-1	21/283=7.4%	45/311=14.4%	7.0
	34372	NG4-1	21/434=4.8%	46/400=11.5%	6.7
UAS-G$_{\gamma}$30A-i	25932	NG4-1	16/319=5.0%	18/286=6.3%	1.3
	34484	NG4-1	9/320=2.8%	31/323=9.6%	6.8
UAS-CaMKI-i	41900	NG4-1	17/337=5.0%	31/328=9.4%	4.4
	35362	NG4-1	10/222=4.5%	17/212=8.0%	3.5
	26726	NG4-1	16/301=5.3%	22/282=7.8%	2.5
UAS-CaMKII-i	35330	NG4-1	49/784=6.2%	91/858=10.6%	4.4
	29401	NG4-1	38/332=11.4%	43/342=12.6%	1.2
UAS-CrebA-i	42526	NG4-1	13/301=4.3%	29/298=9.7%	5.4
UAS-Gprk1-i	35246	NG4-1	13/323=4.0%	15/207=7.4%	3.4

	28354	NG4-1	13/304=4.3%	24/289=12%	7.7
UAS-Gprk2-i	41933	NG4-1	3/218=1.4%	24/228=10.5%	9.1
	35326	NG4-1	12/268=4.5%	35/267=13.1%	8.6
UAS-IP3K-i	35296	NG4-1	10/225=4.4%	14/152=9.2%	4.8
	31733	OR	25/336=7.4%	31/331=9.4%	2.0
	31733	NG4-1	67/572=11.7%	57/555=10.3%	-1.4
UAS-PKC53E-i	34716	NG4-1	18/304=5.9%	22/289=7.6%	1.7
UAS-PKC98E-i	29311	NG4-1	14/293=4.8%	15/284=5.3%	0.5
	35275	OR	9/266=3.4%	25/288=8.4%	5.0
		NG4-1	49/657=7.5%	45/603=7.5%	0.0
	44074	OR	30/597=5.1	36/346=10.4	5.3
		NG4-1	31/289=10.7	38/318=11.9	1.2
UAS-PLC2-i	33719	NG4-1	23/264=8.7%	37/311=11.9%	3.2
UAS-bsk-i	53310	NG4-1	21/380=5.5%	32/346=9.3%	3.8
UAS-Ira-i	31595	NG4-1	6/272=2.2%	8/190=4.2%	2.0
UAS-kay-i	27722	NG4-1	11/256=4.3%	25/259=9.6%	5.3
	31322	NG4-1	22/384=5.7%	61/334=18.3%	12.6
	31391	NG4-1	24/291=8.2%	29/218-13.3%	5.1
UAS-rl-i	36059	NG4-1	21/269=7.8%	32/297=10.8%	3.0
UAS-wt-5-HT1A	27630	NG4-1	16/335=4.8%	30/302=10%	5.2
	27631	NG4-1	10/240=4.2%	24/271=8.9%	4.7
UAS-wt-CrebB17A	7220	NG4-1	51/636=8.0%	98/628=15.6%	7.6
	9232	NG4-1	32/637=5.0%	84/592=14.2%	9.2

UAS-wt-CaMK2R3	29662	NG4-1	20/292=6.8%	28/289=10.0%	3.2
UAS- CaMKII.T287A	29663	NG4-1	16/287=5.6%	25/283=8.8%	3.2
UAS-wt-Gαs	6489	NG4-1	32/289=11.1%	39/300=13.0%	1.9
	6489	NG4-1	40/610=6.6%	54/652=8.3%	1.7
UAS-wt-Ira	7216	NG4-1	15/342=4.4%	44/378=11.6%	7.2
UAS-wt-Kay	7213	NG4-1	24/341=7.4%	70/350=20.0%	12.6

Table 3.2. MI^{GSC} from select RNA-*i*-lines directed against GPCRs

UAS-driven expression of RNA-*i* for the listed GPCRs i via *NG4-1* did not block the increase in MI^{GSC} in response to mating. BL #: Bloomington stock number, Single and Mated: number of pHH3-positive GSCs/total number of GSCs = MI^{GSC}, Diff: MI^{GSC} of mated males minus MI^{GSC} of non-mated males. Note the variability in MI^{GSC} among the different genotypes. GPCRs marked by asterisks were excluded from further studies because their siblings outcrossed to *wt* did not show a stronger response to mating than the experimental (GPCR-*i*/*NG4-1*) flies.

GPCR	BL #	Single	Mated	Diff.
UAS-5-HT2A-i	31882	25/490=5.1	36/465=7.3	2.2
	56870	19/582=3.3	32/553=5.8	2.5
UAS-5-HT2B-i	60488	6/261=2.3	21/272=7.7	5.4
	25874	4/228=1.7	34/236=14.4	12.7
UAS-Ado-R-i	27536	11/276=4.0	20/209=9.6	5.6
UAS-AKHR-i	29577	23/492=4.7	54/574=9.4	4.7
UAS-AR-2-i	25935	13/363=3.6	25/336=7.4	3.6
UAS-CG13229-i	29519	9/285=3.2	33/297= 11.1	7.9

UAS-CG14539-i	25855	21/318=6.6	31/307=10.1	3.5
UAS-CG15556-i	44574	28/425=6.6	43/401=10.7	4.1
UAS-CG15744-i	28516	18/279=6.4	27/252=10.7	4.3
	42497	23/323=7.1	36/236=11.0	3.9
UAS-CG30106-i	27669	10/244=4.1	34/273=12.4	8.3
UAS-CG33639-i	28614	32/300=10.7	47/371=12.7	2.0
*UAS-CCHaR1-i**	51168	27/407=6.6	27/323=8.4	1.8
UAS-Cry-i	43217	43/389=11.0	75/521=14.4	3.4
UAS-CrzR-i	52751	14/337=4.2	31/333=9.3	5.1
UAS-Dop1R1-i	62193	12/352=3.4	25/308=8.1	4.6
	55239	11/300=3.7	44/267=16.5	12.8
UAS-GABA BR2-i	50608	6/176=3.4	35/207=16.9	13.5
	27699	7/291=2.4	18/282=6.4	4.0
UAS-GABA BR3-i	42725	10/190=5.3	28/243=11.5	6.2

UAS-Moody-i	36821	5/301=1.7	16/234=6.8	5.1
UAS-Mth-l1-i	41930	11/279=4.0	42/300=14.0	10
UAS-Mth-l3-i	41877	54/817=6.6	81/850=11.8	5.2
	36822	19/231=8.2	39/241=16.2	8.0
UAS-Mth-l8-i	36886	48/933=5.1	70/915 =7.6	2.5
UAS-Mth-l9-i	51695	61/985=6.2	82/910 =9.0	2.8
UAS-Mth-l15-i	28017	14/349=4.0	25/337=7.1	3.1
UAS-PK1R-i	27539	28/478=5.9	37/375=9.9	4.0
UAS-Smo-i	27037	12/263=4.6	33/288=11.4	6.8
	43134	19/274=7.0	15/147=10.2	3.2
UAS-Tre1-i	34956	5/234=2.1	28/252=11.1	9.0
*UAS-TKR86D-i**	31884	31/564=5.5	28/394=7.1	1.6
UAS-TKR99D-i	55732	30/506=5.9	49/467=10.5	4.6
	27513	4/240=1.7	30/294=10.2	8.5

Table 3.3. MI^{GSC} from additional RNA*i*-lines with modified expression of the GPCRs blocking the increase in MI^{GSC} in mated males

BL #: Bloomington stock number, Single and Mated: number of pHH3-positive GSCs/total number of GSCs = MI^{GSC}, Diff: MI^{GSC} of mated males minus MI^{GSC} of non-mated males.

GPCR	BL #	Single	Mated	Diff.
5HT-1A-i/NG4-1	25834	64/841=7.6	67/777=8.6	1
5HT-1B-i/NG4-1	25833	16/256=6.2	26/268=9.7	3.5
	27635	3/304=1.0	27/317=8.5	7.5
	51842	20/381=5.2	32/375-8.5	3.3
	54006	13/405=3.2	23/351=6.5	3.3
5HT-7-i/NG4-1	32471	8/238=3.4	17/229=7.4	4.0
CG12290-i/NG4-1	42520	4/260=1.5	31/246=12.6	11.1
Mth-i/NG4-1	27495	14/352=4	15/336=4.5	0.5

Table S3.1. Fertility Assay

Male fertility was calculated based on the % of females that produced offspring after mating with males of the indicated genotype. BL#: Bloomington stock number.

Genotype	BL #	Male fertility
OR	N/A	72%
CS	N/A	62%
5HT-1A-i /NG4-1	33885	75%
5HT-1B-i /NG4-1	33418	61%
5HT-7-i/NG4-2	27273	91%
CG12290-i /NG4-1	31873	77%
Mth-i /NG4-1	36823	90%
Mth-l5-i /NG4-1	42515	84%
Octβ2R-i /NG4-1	50580	89%
$5HT\text{-}1A^{\Delta 5kb}$ /$5HT\text{-}1A^{\Delta 5kb}$	27640	15%
$5HT\text{-}1B^{\Delta III\text{-}V}$ /$5HT\text{-}1B^{\Delta III\text{-}V}$	55846	30%

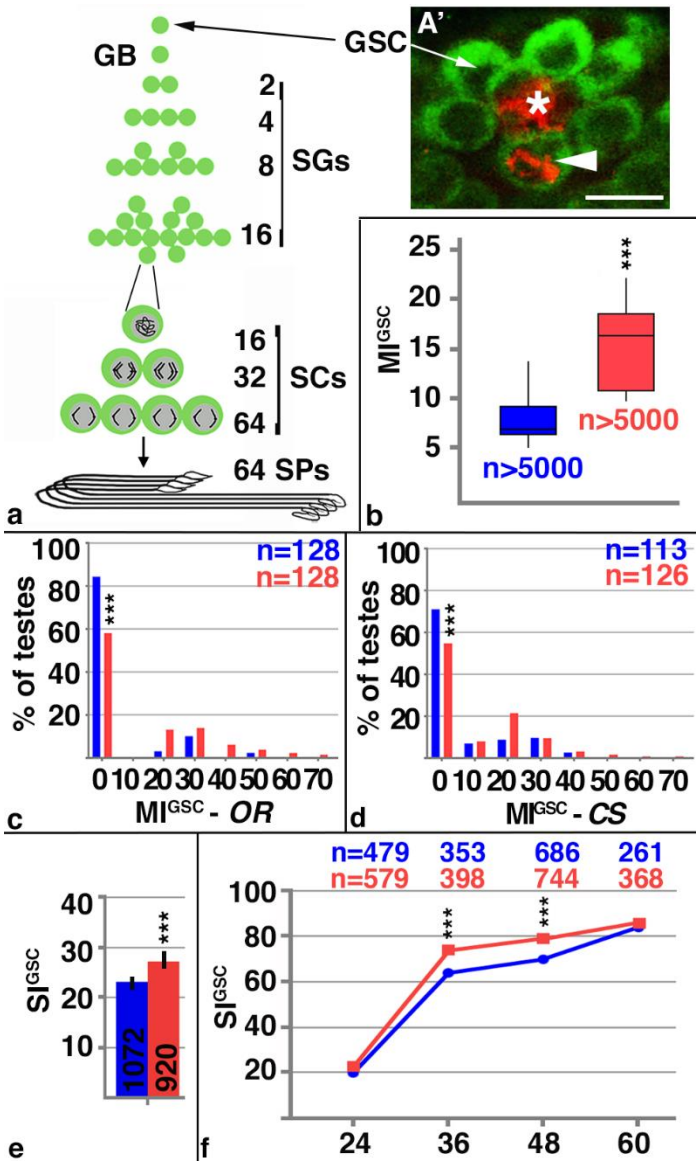

Figure 3.1. Mating increased male stem cell division frequency.

A) Cartoon depicting the stages of *Drosophila* spermatogenesis. Note that every GSC division produces exactly 64 spermatids. GB: gonialblast, SG: spermatogonia, SC: spermatocytes, SP: spermatids.

A') The apical tip of a *wt* testis. The FasIII-positive hub (asterix) is surrounded by seven Vasa-positive GSCs (green), one of which is in mitosis based on anti-pHH3-staining (arrowhead). Scale bar: 10μm.

B-F) Blue: non-mated condition, red: mated condition, ***: P-value < 0.001, numbers of GSCs and number of gonads (n=) as indicated.

B) Box plots showing the range of MI^{GSC}. Lines within boxes represent medians, whiskers represent outliers.

C, D) FDGs showing bin of MI^{GSC} (bin width=10) across a population of c) *OR* and D) *CS* males on the X-axis and the percentage of testes with each MI^{GSC} on the Y-axis.

E) Bar graph showing SI^{GSC} of *OR* males from three independent experiments.

F) Graph showing the percentage of EdU-marked *OR* GSCs on the Y-axis and hours of feeding and mating on the X-axis.

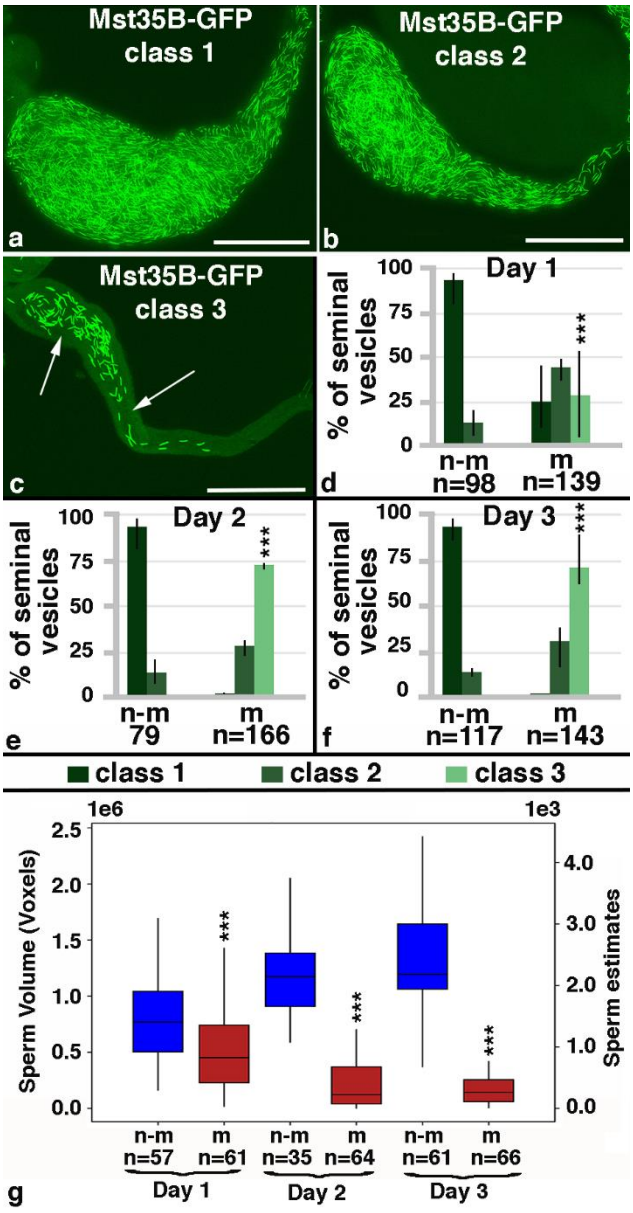

Figure 3.2. Mating reduced the mature sperm pool.

A-C) Class 1,2 and 3 seminal vesicles from Mst35B-GFP males. Scale bars: 0.1 mm; arrows point to GFP-negative regions.

D-G) Numbers of seminal vesicles (n=) as indicated, n-m: non-mated, m: mated, ***: P-value < 0.001.

D-F) Bar graphs showing the distribution of Class 1 to 3 seminal vesicles in non-mated and mated males at days one to three of the mating experiment. Three fly lines that carry GFP-marked sperm were used: one that carries Dj-GFP (BL#5417), one that carries the Mst35B-GFP (BL#58408), and one line that carries both constructs (BL#58406).

G) Box plot showing sperm head volume (based on MST35B-GFP) per seminal vesicle in non-mated and mated males on days one to three of the experiment.

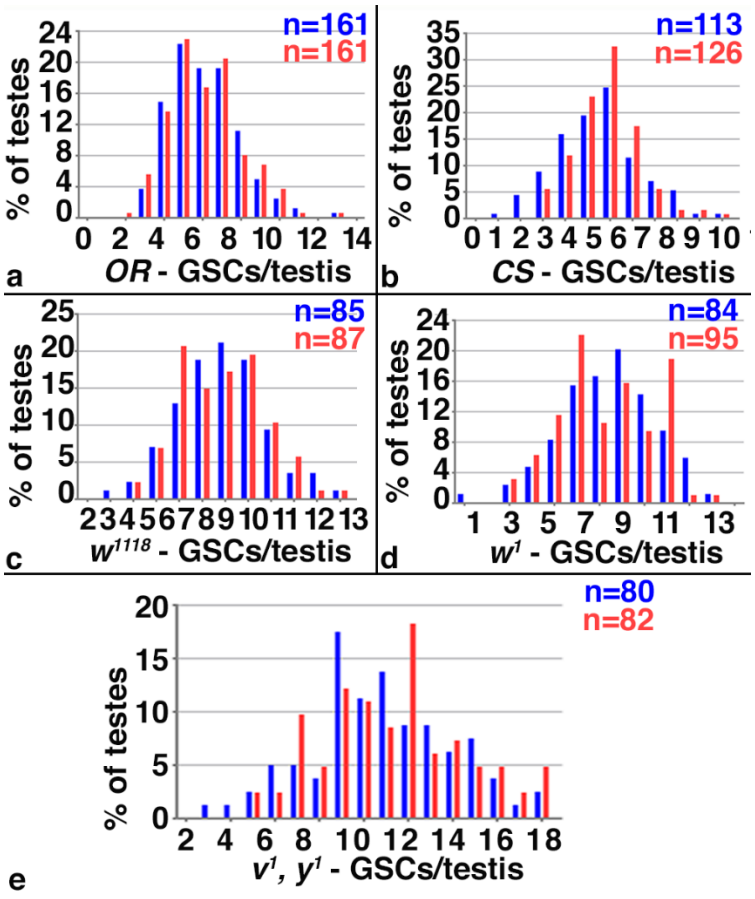

Figure 3.3. Mating did not affect GSC numbers.

A-E) Blue: non-mated condition, red: mated condition, numbers of gonads (n=) as indicated, genotypes as indicated.

A-E) FDGs showing numbers of GSCs on the X-axis and percentage of testes with the number of GSCs on the Y-axis. No difference in GSC numbers was observed between non-mated and mated males from different genetic backgrounds.

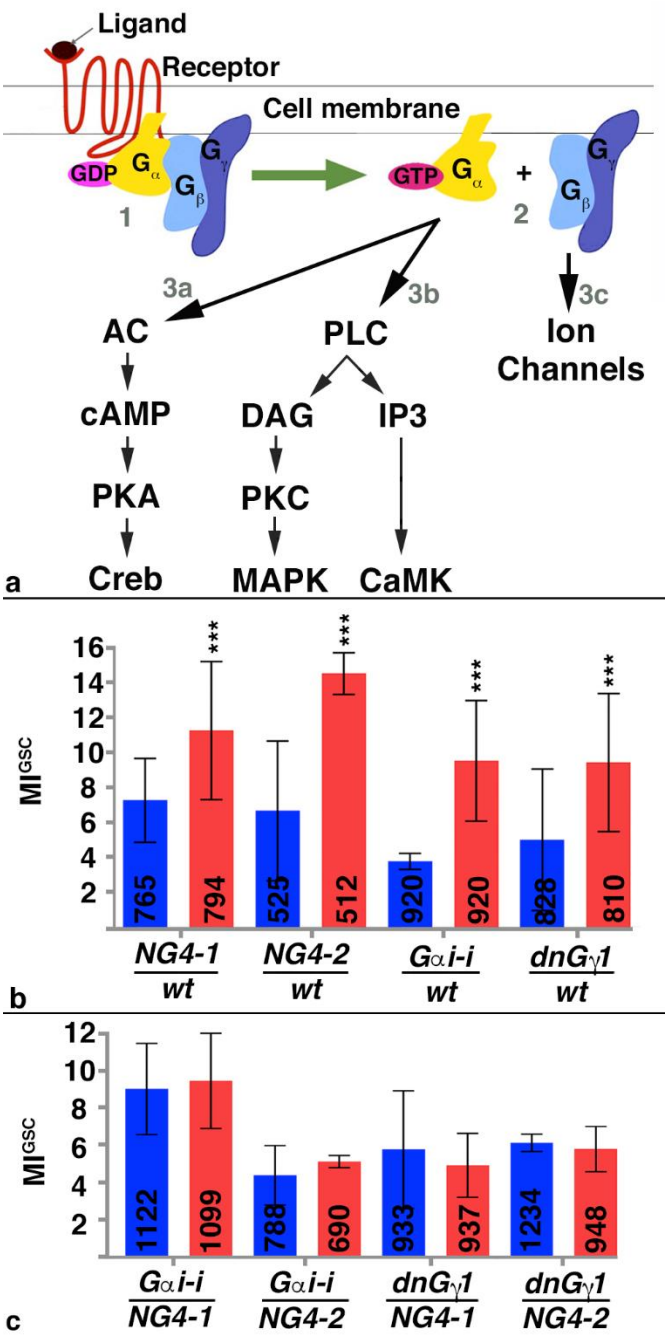

Figure 3.4. G-proteins were required for the increase in MI^{GSC} in response to mating.

A) Cartoon depicting the activation of G-proteins upon GPCR stimulation by ligand. 1: G-protein association before GPCR stimulation, 2: G-protein

distribution after GPCR stimulation, 3a-c: downstream signaling cascades. AC: Adenylyl Cyclase, cAMP: cyclic Adenosine Monophosphate, PKA: Protein Kinase A, CREB: cAMP responsive element-binding protein, PLC: Phospho Lipase C, DAG: Diacylglycerol, PKC: Protein Kinase C, MAPK: Map Kinase, IP3: Inositol Triphosphate, CaMK: Calcium^{2+}/calmodulin-dependent protein kinase.

B, C) Bar graphs showing MI^{GSC}. Blue: non-mated condition, red: mated condition, ***: P-value < 0.001, numbers of GSCs as indicated, genotypes as indicated.

B) Control animals increased MI^{GSC} in response to mating.

C) Males expressing *$G_{\alpha}i$-i* or dnG_{γ}1 in the germline did not increase MI^{GSC} after mating.

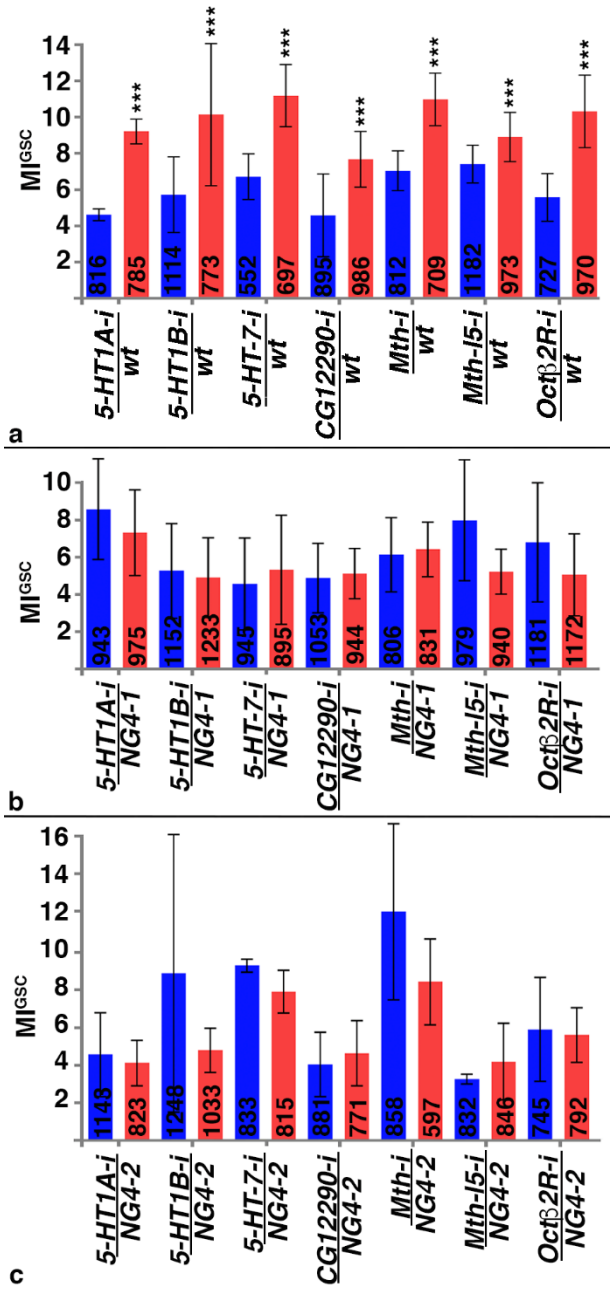

Figure 3.5. Expression of RNA-*i* against seven distinct GPCRs blocked the increase in MI^{GSC} in response to mating.

A-C) Bar graphs showing MI^{GSC}. Blue: non-mated condition, red: mated condition, ***: P-value < 0.001, numbers of GSCs as indicated, genotypes as indicated.

A) Control males have significantly higher MI^{GSC} than their non-mated siblings. B, C) Mated (B) *GPCR-i*/NG4-1 and (C) *GPCR-i*/NG4-2 males did not have significantly higher MI^{GSC} compared to their non-mated siblings.

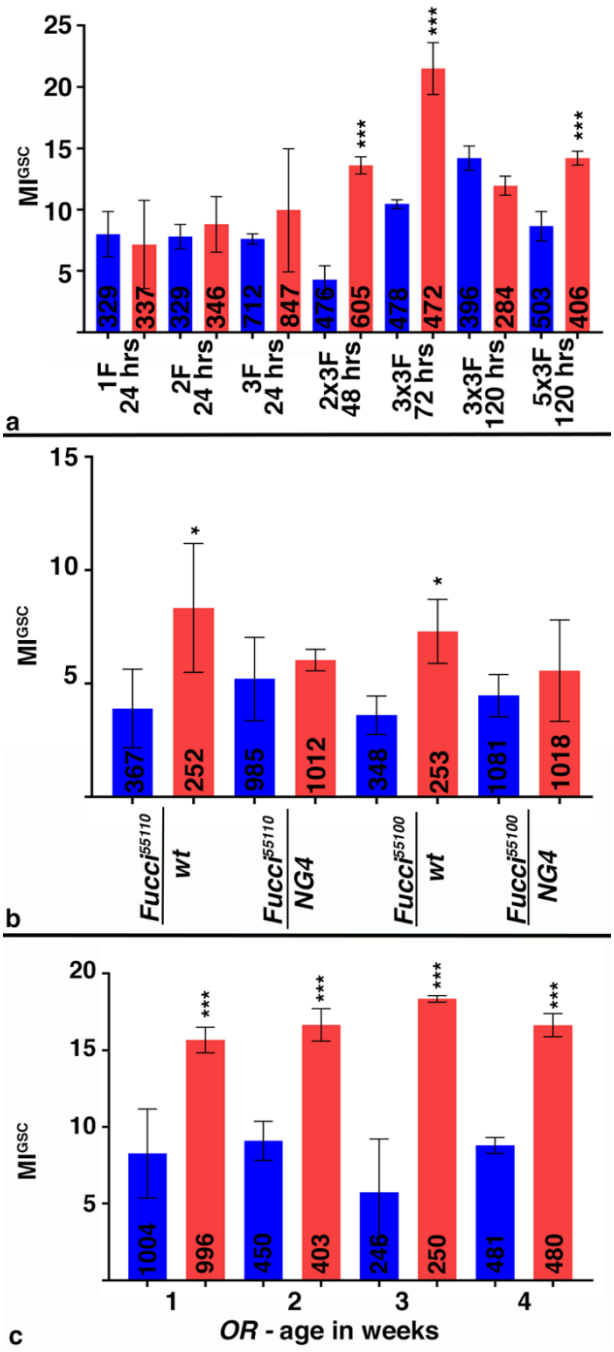

Figure S3.1. Validation of mating conditions for the increase in MI^{GSC}.

A-C) Bar graphs showing MI^{GSC}. Blue: non-mated condition, red: mated condition, ***: P-value < 0.001, *: P-value < 0.05, numbers of GSCs as indicated, genotypes as indicated.

A) MI^{GSC} after different mating conditions, as indicated. F: female virgins, hrs: hours.

B) MI^{GSC} from experimental (*Fucci/NG4*) and control (*Fucci/wt*) Fucci-lines.

C) MI^{GSC} of non-mated and mated *OR* males at one, two, three, and four weeks of age.

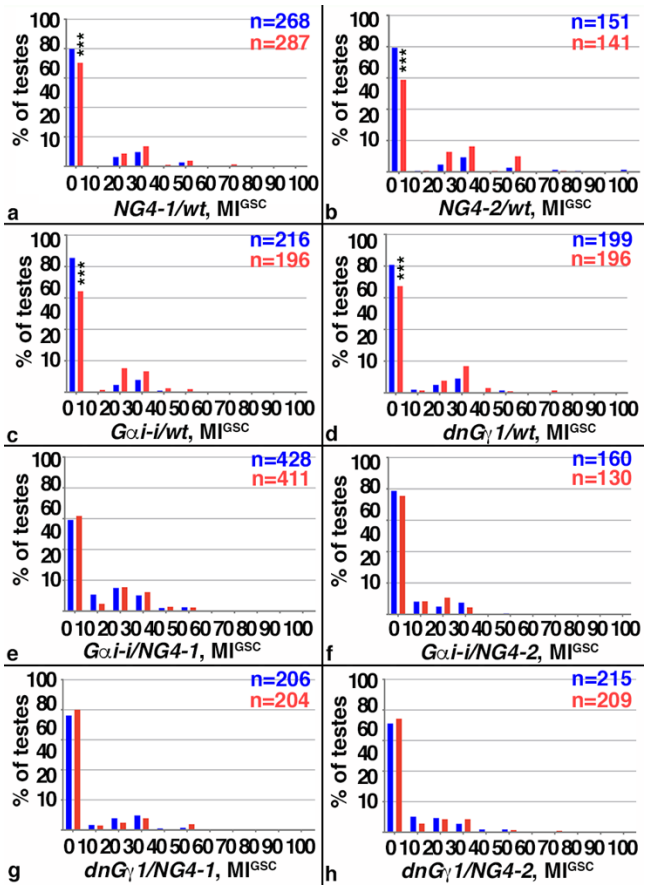

Figure S3.2. Modulated G-protein did not significantly change the distribution of MIGSC across the population of testes.

A-H) FDGs showing median of bin of MI^{GSC} across populations of males on the X-axis (bin width=10) and the percentage of testes with each MI^{GSC} on the Y-axis. Blue: non-mated condition, red: mated condition, n: number of testes examined, genotypes as indicated, ***: P-value < 0.001.

A-D) Control males

E-H) Males expressing $G_{\alpha}i$-i or $dnG_{\gamma}1$ in the germline.

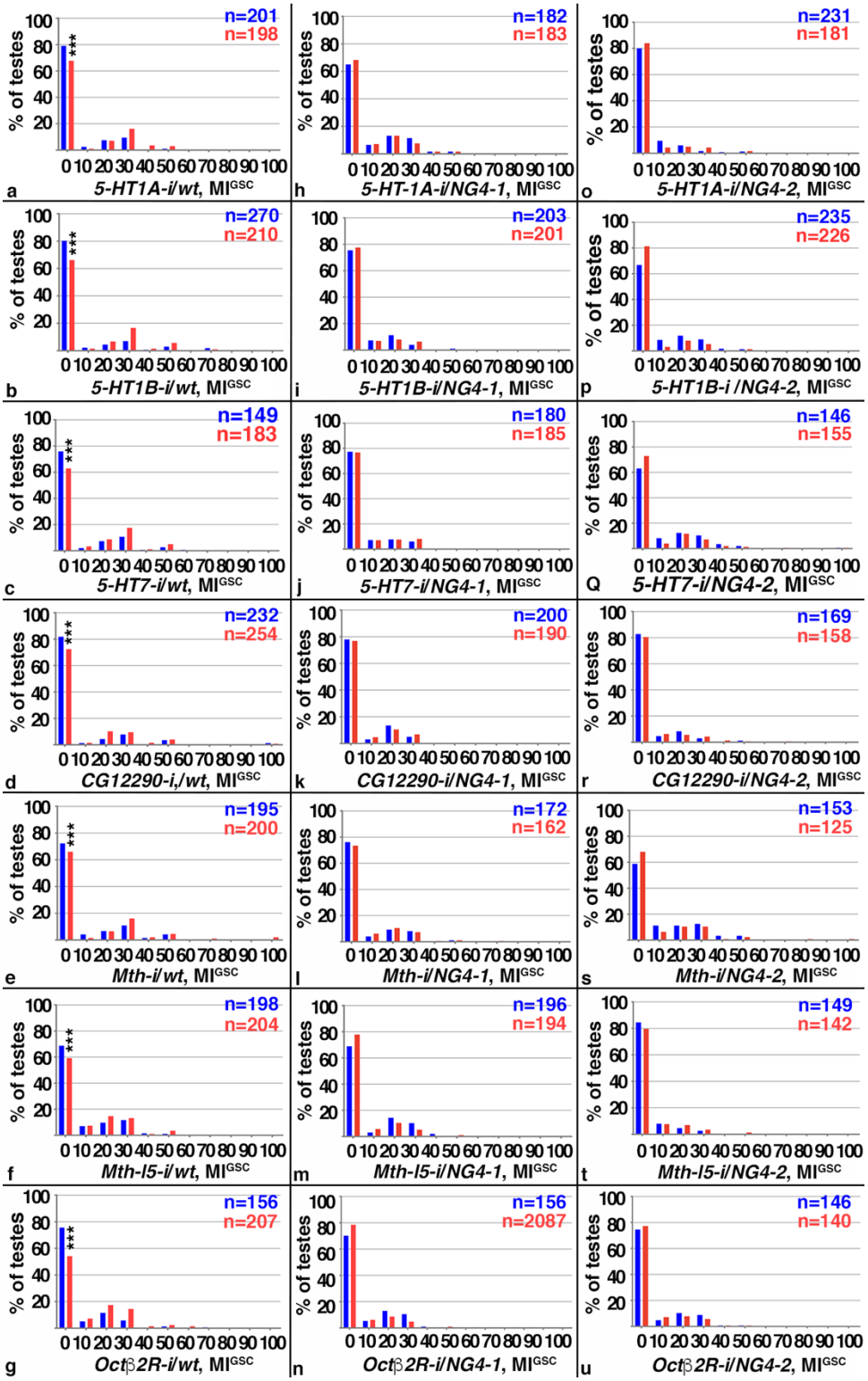
% of testes
0 10 20 30 40 50 60 70 80 90 100
***
a n=201 n=198 5-HT1A-i/wt, MI^GSC
h n=182 n=183 5-HT-1A-i/NG4-1, MI^GSC
o n=231 n=181 5-HT1A-i/NG4-2, MI^GSC
b n=270 n=210 5-HT1B-i/wt, MI^GSC
i n=203 n=201 5-HT1B-i/NG4-1, MI^GSC
p n=235 n=226 5-HT1B-i /NG4-2, MI^GSC
c n=149 n=183 5-HT7-i/wt, MI^GSC
j n=180 n=185 5-HT7-i/NG4-1, MI^GSC
Q n=146 n=155 5-HT7-i/NG4-2, MI^GSC
d n=232 n=254 CG12290-i,/wt, MI^GSC
k n=200 n=190 CG12290-i/NG4-1, MI^GSC
r n=169 n=158 CG12290-i/NG4-2, MI^GSC
e n=195 n=200 Mth-i/wt, MI^GSC
l n=172 n=162 Mth-i/NG4-1, MI^GSC
s n=153 n=125 Mth-i/NG4-2, MI^GSC
f n=198 n=204 Mth-l5-i/wt, MI^GSC
m n=196 n=194 Mth-l5-i/NG4-1, MI^GSC
t n=149 n=142 Mth-l5-i/NG4-2, MI^GSC
g n=156 n=207 Octβ2R-i/wt, MI^GSC
n n=156 n=2087 Octβ2R-i/NG4-1, MI^GSC
u n=146 n=140 Octβ2R-i/NG4-2, MI^GSC

Figure S3.3. No change in the distribution of MI^{GSC} in response to mating was seen upon expressing RNA-*i* against seven of the GPCRs.

A-U) FDGs showing median of bin of MI^{GSC} across populations of males on the X-axis (bin width=10) and the percentage of testes with each MI^{GSC} on the Y-axis. Blue: non-mated condition, red: mated condition, n; number of testes examined, genotypes as indicated, ***: P-value < 0.001.

A-G) Control males.

H-U) Males expressing RNA-*i* against seven GPCRs in the in the germline via (H-N) *NG4-1* or (O-U) *NG4-2*.

CHAPTER 4

DISCUSSION

This thesis explores the male germline, taking advantage of two model systems; the mouse and *D. melanogaster*. The fruit fly provides increased investigative power and screening potential through easy rearing and high populations. While the mouse lends closer ties to humans occupying the same taxonomic class.

In chapter 2 we adopt a tissue clearing technique paired with light-sheet microscopy to examine the undifferentiated spermatogonia in relation to the complex mammalian testis architecture. This is the first use of such an approach in the adult mouse gonad. We began by demonstrating the efficacy of such an approach, having adopted new technologies. This was accomplished by comparing volumes covering the top, middle, and bottom regions of an image stack encompassing the short axis of a testis. Next, we asked if structural characteristics of the testis tissue could be assessed. The seminiferous cycle was broadly measured by relating bright and dim population fluctuations to the seminiferous tubule axis. We further show that populations could be related to the interstitial niche using an automated analysis. Finally, we show this technology is suitable for examination of putative stem cell populations achieving semi-automated characterization GFRα1. We also are able to label for GFP-positive ID4 expressing cells.

Having demonstrated the ability to image cleared testis tissue, many potential future uses for this technology exist. Being able to rapidly process samples in parallel for efficient imaging promises a pipeline capable of handling large power studies. This approach is further aided by computer analysis and signal recognition. While signal heterogeneity, resultant from tissue variation poses a challenge, methods of image correction are being developed. The comparison of cell populations and how they change in mutant conditions could be rapidly examined. Furthermore, it has long been understood that environmental conditions can have drastic effects on spermatogenesis from temperature sensitivity to chemical perturbation. Much of the field have sought a culture system to examine such factors. Tissue clarification and light-sheet microscopy could be utilized as a part of a screening pipeline making us of an animal model.

Much of the technology has been developed for the neuroscience community. One innovative approach in the brain has been the utilization of tissue clearing for intact tissue single-cell RNA sequencing[1]. Such a method in mammalian germline could greatly assist in our understanding of the heterogeneity present in spermatogonia. Furthermore, transcriptomes from several groups have been published and serve as an excellent database for exploration[2–4].

Chapter 3 of this thesis looks at the effect of mating on germline stem cells (GSCs) using the genetically tractable fruit fly. We observe an increase in the mitotic index and S-phase index of wild-type germline after three successive

days of mating. The overall size of the GSC population remained the same regardless of mating status. Intuitively, such an increase could be in response to usage of the downstream sperm. Thus we utilized lines with GFP-labeled sperm to ensure this was the case. Both qualitative classification and computer quantitated volumes of sperm heads within the seminal vesicle showed a reduction of gamete pool.

While the mitotic increase was not confined to the GSC population, the rest of the chapter takes focus on this population. We used a screening approach to isolate factors involved in increased mitotic index utilizing easily obtained RNA-*i* stocks. After observing a lack of mitotic response to mating in several RNA-*i*-lines directed against G-proteins we found that this is also the case when expressing a dominant negative $G_{\gamma}1$. This caused us to investigate G-protein coupled receptors (GPCRs). Using the same RNA-*i* screening procedure we found seven receptors that also failed to produce a mating phenotype (5HT-1A, 5HT-1B, 5HT-7, MTH, MTH-I5, OCTβ2R, and CG12290).

Future directions of this project would require understanding the G-protein pairings of each of the above GPCRs as most of these interactions have gone uncharacterized. GPCRs in particular pose the challenge of potentially pairing with multiple combinations of the heterotrimeric G-protein subunits. In mammals G_{α} proteins are linked to specific response elements and are thusly classified into subgroups[5]. $G_{\alpha}s$, $G_{\alpha i}i/o$, $G_{\alpha}q$, and $G_{\alpha}12/13$ ultimately operate on cAMP response element (CRE), serum response element (SRE), nuclear factor of activated T-cells response element (NFAT-RE), and serum response factor response

element (SRF-RE) respectively. These subgroups are conserved in the 6 G_α subunits present in *Drosophila* with exception of G_αf being specific to invertebrates[6–8]. Each receptor could be expressed in an *in vitro* system and with response element reporters to further examine the relationship between G-protein and GPCR. Characterization of these GPCRS could yield insight into how seven receptors all act on germline mitotic activity.

Germline represents the future of a species. The necessity of understanding the intricacies of the cells in which all of us arise requires no validation. Even so, recent reports have demonstrated that some manner of perturbation is occurring. Whether environmental or evolutionary, the overall production of sperm is on the decline in the western male, and potentially across demography[9]. Furthermore, life-saving treatment for cancer can leave an adolescent without the potential to produce offspring. It has never been clearer that our understanding must be furthered.

References:

1. Wang, X. *et al.* Three-dimensional intact-tissue sequencing of single-cell transcriptional states. *Science (80-.).* **361**, (2018).
2. Green, C. D. *et al.* A Comprehensive Roadmap of Murine Spermatogenesis Defined by Single-Cell RNA-Seq Data Resources GSE112393 Green et al. *Dev. Cell* **46**, 651–667 (2018).
3. Lukassen, S., Bosch, E., Ekici, A. B. & Winterpacht, A. Characterization of germ cell differentiation in the male mouse through single-cell RNA sequencing OPEN. *Sci. Rep.* **8**, 6521 (2018).
4. Hermann, B. P. *et al.* The Mammalian Spermatogenesis Single-Cell Transcriptome, from Spermatogonial Stem Cells to Spermatids. *Cell Rep.* **25**, 1650-1667.e8 (2018).
5. Wettschureck, N. & Offermanns, S. Mammalian G proteins and their cell type specific functions. *Physiological Reviews* vol. 85 1159–1204 (2005).
6. Hearn, M. G. *et al.* A Drosophila dopamine 2-like receptor: Molecular characterization and identification of multiple alternatively spliced variants. *Proc. Natl. Acad. Sci. U. S. A.* **99**, 14554–14559 (2002).
7. Jonchère, V. *et al.* Transcriptional responses to hyperplastic MRL signalling in Drosophila. *Open Biol.* **7**, (2017).
8. Katanayeva, N., Kopein, D., Portmann, R., Hess, D. & Katanaev, V. L. Competing activities of heterotrimeric G proteins in Drosophila wing maturation. *PLoS One* **5**, (2010).
9. Levine, H. *et al.* Temporal trends in sperm count: a systematic review and

meta-regression analysis. *Hum. Reprod. Update* **23**, 646–659 (2017).